consists of performing an analysis for a particular experimental facility for a specific transient test. The results from a RELAP5 simulation of the test are compared against measurements from the experiment and conclusions are drawn regarding the code capabilities for predicting the physical behavior of the test.

Prior assessments of RELAP5 have been performed for a wide variety of transients over the 20-year development history of the code. Many of those assessments focused on tests representing LOCAs, for which the key system response is the integrity of the reactor core. It is noted that LOCAs as an event category are also an important vessel failure risk contributor for PTS, and so the extensive LOCA experimental database remains relevant and very useful for PTS applications. However, in contrast to the focus on core behavior during LOCAs, the focus for PTS-related transients is on the temperature and pressure conditions in the reactor vessel downcomer. Hence, the assessments discussed here focus on comparing RELAP5 results to experimental data for conditions in the downcomer.

The assessment of RELAP5/MOD3.2Gamma for representing PTS behavior, performed in the context of the PIRT discussion presented in Section 6.2, are summarized in the following sections. The assessments are documented in detail in the RELAP5 PTS Assessment Report [*Fletcher*].

6.7.1 Separate Effects Tests

RELAP5 was assessed against separate-effects experiments to evaluate RELAP5 capabilities for predicting specific localized behavior that is relevant for PTS. These separate-effects experiments included Marviken tests for assessing critical flow models, MIT pressurizer facility tests for assessing steam condensation and RCS pressurization behavior, UPTF full-scale tests for assessing condensation and steam-water flow phenomena and semiscale tests for assessing coolant loop natural circulation flow behavior. These assessments are discussed in this section.

6.7.1.1 Marviken Tests

Critical flow assessments were performed using data obtained from two experiments conducted at the Marviken facility. Marviken is a full-scale test facility fabricated from the 14,830-ft^3 (420-m^3) pressure vessel that was part of the Marviken nuclear power plant. RELAP5 is assessed against Marviken Tests 22 and 24.

During the experiments, the vessel is pressurized, the desired temperatures and liquid levels are established, and the break is opened, allowing a blowdown of the vessel to occur through a discharge pipe. The two tests differ mainly in the length of the discharge pipe that is employed.

The RELAP5 code utilizes the Henry-Fauske critical flow model to determine the break flow rate during periods when critical flow occurs.

A comparison of the measured and RELAP5-calculated vessel discharge flow rates for Marviken Test 22 is presented in Figure 6.6. The RELAP5 prediction of mass flow rate is in excellent agreement with the test data. The comparison of results for Test 24 is similar.

The Marviken assessments indicate that RELAP5 is capable of predicting critical break flow in an experimental system of the prototype scale. However, issues related to the exact configuration of breaks in PWR piping result in an additional general break flow prediction uncertainty. In order to account for this general uncertainty, the PTS plant calculations were performed using a spectrum of break diameters and locations. Break diameters from 1-in. (2.54-cm) to 22.63-in. (57.5-cm) in equal flow area increments were analyzed in the PTS plant evaluations.

6.7.1.2 MIT Pressurizer Test ST4

The MIT test facility is a small-scale, low-pressure representation of a PWR pressurizer. The insulated test vessel is 3.74-ft (1.14-m) tall with an inner diameter of 0.667-ft (0.203-m). Test ST4 was initialized with 1.41-ft (0.432-m) of saturated water in the bottom of the vessel at

a pressure of 0.493 MPa [71.5 psia]. During the test, subcooled water is injected into the bottom of the vessel, increasing both the water level and pressure.

The capabilities of RELAP5 for simulating the steam condensation and the interfacial heat transfer between the stratified liquid and the vapor above the liquid were tested using comparisons to the measured data from this test. The mixing of the cold incoming water with hot water initially in the tank affects the prediction of the pressure increase, which for PTS is an important phenomenon. The simulation of this test is included in the set of standard problems that is executed routinely for RELAP5 developmental assessment.

A comparison of the measured and RELAP5-calculated pressure behavior is shown in Figure 6.7. The pressure increases as a result of the compression of the steam volume above the water surface. As the pressure increases, so too does the saturation temperature, leading to condensation of steam on the tank walls and liquid interface. RELAP5 predicted the trend of the pressure increase well, but somewhat

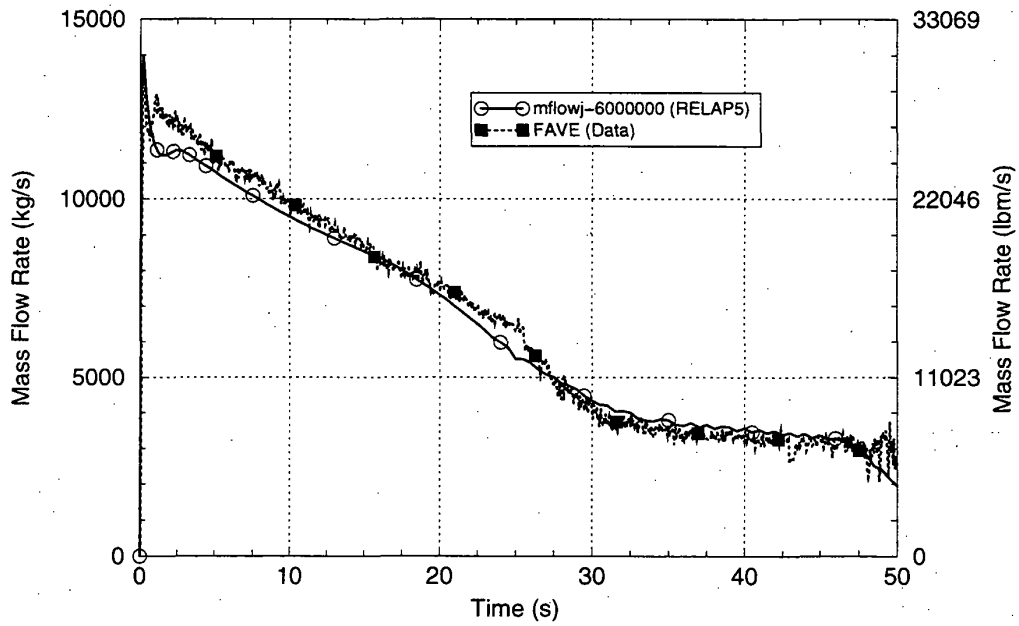

Figure 6.6. Mass Flow Rate at Nozzle Outlet (Marviken Test 22)

overpredicted the pressure. The pressure overprediction is attributed to an underprediction of the environmental heat losses with the model. Heat losses in a small facility like the MIT test facility can have a significant impact on system parameters such as pressure. Overall, the assessment indicates that RELAP5 is capable of well-predicting the pressure increases experienced when steam regions within the RCS of a PWR are compressed.

6.7.1.3 Upper Plenum Test Facility

The Upper Plenum Test Facility (UPTF) is a full-scale model of a four-loop 1,300 MWe PWR. Components included in this facility are the reactor vessel, downcomer, lower plenum, core simulator, upper plenum, and four coolant loops, each with reactor coolant pump and steam generator simulators. The test vessel, core barrel, and internals are a full-size representation of a PWR reactor vessel.

RELAP5 assessment was performed for Run 131 of UPTF Test 6. This test represents the interaction of steam and water in the reactor vessel downcomer and lower plenum regions of a PWR during the end-of-blowdown and refill portions of a large cold-leg break LOCA. The test investigates the behavior as the ECC water injected into the cold legs penetrates downward into the reactor vessel downcomer.

The test is run by injecting steam at a constant rate through the core and steam generator simulators at pressure and temperature conditions of 0.258 MPa [37.4 psia] and 458 K (364°F). The steam flows in the reverse direction, upward through the reactor vessel downcomer, toward the broken cold leg. When the steam flow behavior becomes steady, slightly subcooled emergency core cooling water at 392 K [246°F] is injected into the cold legs of the three intact loops.

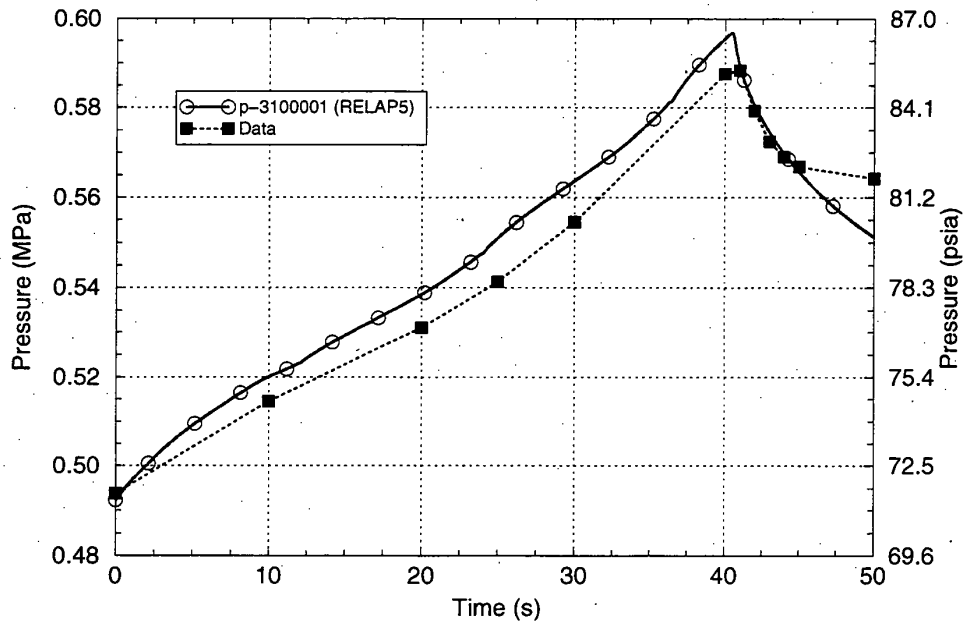

Figure 6.7. Pressure Rise (MIT Pressurizer Test ST4)

The RELAP5 simulation for UPTF Test 6, Run 131 indicates that the code well-predicts the measured downcomer pressure, lower plenum liquid level, and downcomer fluid temperature responses during the test. RELAP5 under predicted the downcomer fluid temperature by an average of 8 K (15°F) over the test period.

6.7.1.4 Semiscale Tests

Experiments were performed in the Semiscale Mod-2A test facility to evaluate single-phase, two-phase, and reflux steady-state coolant loop natural circulation behavior. This facility is a small-scale model of the primary coolant system of a four-loop PWR. The scaling factor between the test facility and full-scale plant is 1:1705. Two Semiscale Mod-2A tests, S-NC-2 and S-NC-3, are used for RELAP5 assessment.

The test facility represents the major components of a PWR, including, steam generators, reactor vessel, downcomer, reactor coolant pumps, pressurizer, and loop piping. The natural circulation experiments conducted at the facility utilized a single-loop configuration where the intact loop pump was replaced with a

spool piece containing an orifice that simulated the hydraulic resistance of a locked pump rotor. The reactor vessel was also modified for these experiments to ensure a uniform heatup of the entire system and to avoid condensation in the vessel upper head region.

In Test S-NC-2, the steady-state loop natural circulation flow rate is measured as a function of the primary-side mass inventory. Single-phase, two-phase, and reflux steady-state modes were examined by varying the primary-side system mass while holding the SG secondary side conditions constant. During the test, a total of 17 separate steady-state conditions with different primary-side inventories ranging from 100 % to 61.2% of the full or maximum inventory were evaluated.

The RELAP5-calculated loop flow rates for Test S-NC-2 compare well with the test data for primary system inventories above 97% (single-phase liquid circulation and low-void two-phase circulation) and below 70% (reflux cooling circulation). For two-phase loop circulation, RELAP5 tended to overpredict the measured circulation rate for inventories between 70% and 90% and to underpredict it for inventories between 90% and 97%. The disagreement between the calculated and measured flow rates for inventories between 70% and 97% is attributed to overprediction of interphase drag by RELAP5.

In Test S-NC-3, the SG secondary side inventory is varied and the primary-side natural circulation flow rate is measured as a function of the reduced effective SG heat transfer area. As the SG inventory declines, the SG heat removal capability and the driving potential for primary-side loop circulation (the density difference between the core and the SG) is diminished, causing the primary flow rate to decline.

RELAP5 well-predicted the measured primary-side flow at effective SG heat transfer areas above 55% but overpredicted the primary-side flow at lower inventories.

In summary, RELAP5 well-predicted the two semiscale natural circulation tests for the conditions associated with high primary- and secondary-side coolant system inventories. The code also well-predicted the transitions to lower primary-side flow rates resulting from reduced primary- and secondary-side inventories. However, at reduced primary- and secondary-side inventories, the code generally tended to overpredict the primary-side flow rate and these overpredictions are believed to result from an overprediction of interphase drag.

Overpredicting the primary-side flow rate generally is nonconservative from the viewpoint of PTS analysis. Since the temperature of the coolant loop flow typically is much higher than the ECCS injection temperature, faster loop flows result in warmer temperatures for coolant entering the reactor vessel. The assessments indicate that under degraded inventory conditions, the primary-side flow rate may be overpredicted by a factor of about two. The maximum downcomer fluid temperature uncertainty that results from overpredicting the loop flow is estimated to be 19 K (34°F). However, it is noted that this uncertainty applies only during simulation of event sequences involving natural circulation, and then only during specific time periods within them when the primary or secondary system inventories are degraded. This uncertainty is evaluated as part of the integral system assessments that follow.

6.7.2 Integral System Response

RELAP5 was assessed against integral-effects experiments to evaluate code capabilities for predicting the system response in facilities scaled to pressurized water reactors. The assessments focus on the code capabilities for predicting the behavior of the reactor vessel downcomer conditions, which are of greatest significance for PTS analysis. The integral-effects experiments address phenomena in coolant system configurations specifically representing the geometries of Westinghouse, Combustion Engineering, and Babcock & Wilcox PWR plant designs. The integral-effects tests simulated PWR behavior under conditions expected during small, medium, and large break LOCAs; stuck-open pressurizer SRV events; and feed-and-bleed cooling operation scenarios.

These sequence categories make up the majority of the risk-dominant sequences in the PTS evaluation study for the Oconee-1, Beaver Valley-1 and Palisades PWRs.

The integral tests used in the assessments were performed in the ROSA-IV, ROSA/AP600, OSU-APEX, LOFT, and MIST experimental facilities. Comparisons of pressures and temperatures measured in these experiments to those predicted by RELAP are made in Sections 6.7.2.1 through 6.7.2.5. Section 6.7.2.6 makes comparisons between heat transfer coefficient estimates from these and other experimental data and those predicted by RELAP.

6.7.2.1 ROSA-IV Experiments

The ROSA-IV facility is a 1/48 volume-scaled, full-pressure representation of a Westinghouse 3,423 MWt four-loop PWR. The facility utilizes a full-height electrically heated core. The four PWR coolant loops are represented with two equal-volume loops. Components included in the loops are the hot leg, steam generator, reactor coolant pump, cold leg, pressurizer (on the intact loop) and ECCS systems (HPI, LPI, and accumulators).

RELAP5 was assessed against two ROSA IV experiments, SB-CL-18 and SB-HL-06.

ROSA-IV Test SB-CL-18 represents a 5% 6-in. (15.24-cm) equivalent diameter scaled break on the side of a cold leg with the reactor in full-power operation. The HPI and AFW systems are assumed to fail and a LOOP is assumed to occur at the time of the reactor trip.

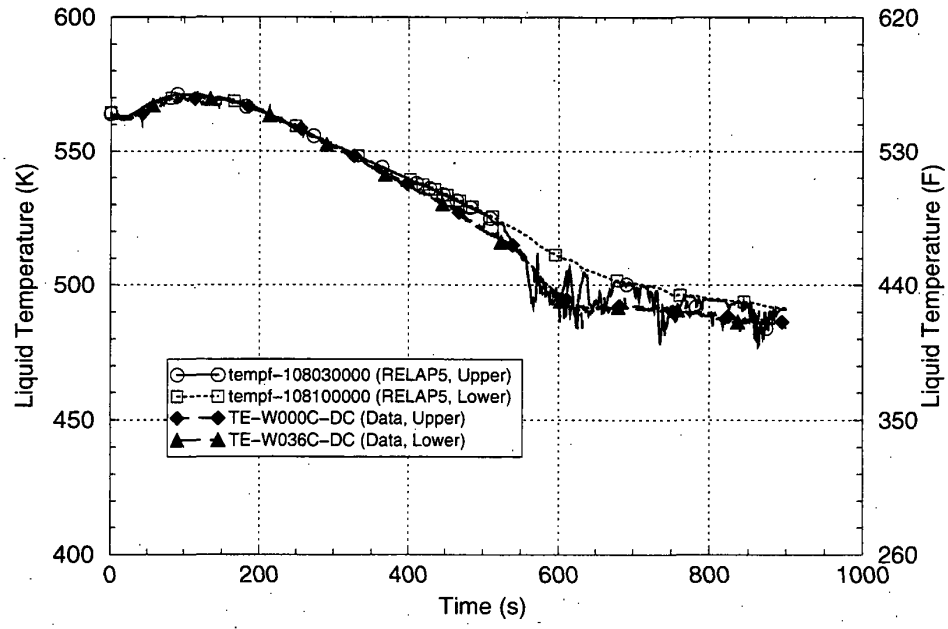

Figure 6.8. Reactor Vessel Downcomer Fluid Temperatures (ROSA-IV Test SB-CL-18)

The assessment of RELAP5 against the test data from ROSA-IV Test SB-CL-18 indicates that the code is capable of acceptably simulating the experiment behavior including the parameters of key importance for PTS (RCS pressure, coolant loop flow, and reactor vessel downcomer temperatures). Figure 6.8 compares the measured and RELAP5-calculated reactor vessel downcomer fluid temperatures. The data shown are for elevations within the downcomer corresponding to the top and bottom of the reactor core. RELAP5 overpredicted the

downcomer fluid temperature by a maximum of 13 K (23°F) and underpredicted it by a maximum of 23 K (41°F). Over the test period, RELAP5 overpredicted the downcomer fluid temperature by an average of 0.16 K (0.29°F).

ROSA-IV Test SB-HL-06 represents a 0.5% 2-in. (5.08-cm) equivalent diameter scaled break on the top of the hot leg with the reactor in full-power operation. The HPI and AFW systems are assumed to fail and a LOOP is assumed to occur at the time of the reactor trip. When the core uncovered and the heatup began, the pressurizer PORV was opened to depressurize the primary system and initiate accumulator injection.

The assessment of RELAP5 against the test data from ROSA-IV Test SB-HL-06 indicates that the code is capable of acceptably simulating the experimental behavior including the parameters of key importance for PTS (RCS pressure, coolant loop flow, and reactor vessel downcomer temperatures). Figure 6.9 compares the measured and RELAP5-calculated reactor vessel downcomer fluid temperatures. The data shown are for elevations within the downcomer corresponding to the top and bottom of the reactor core. The large drop in the measured downcomer temperature at about 8,000 s resulted from a condensation-driven rapid movement of water into the pressurizer; this water movement was not seen in the RELAP5 calculation. Condensation is an expected uncertainty in code calculations and the current state of the art in thermal-hydraulic modeling does not allow accurate predictions of extreme transient condensation events. RELAP5 underpredicted the downcomer fluid temperature by a maximum of 70 K (126°F) and by an average of 10 K (18°F) over the test period.

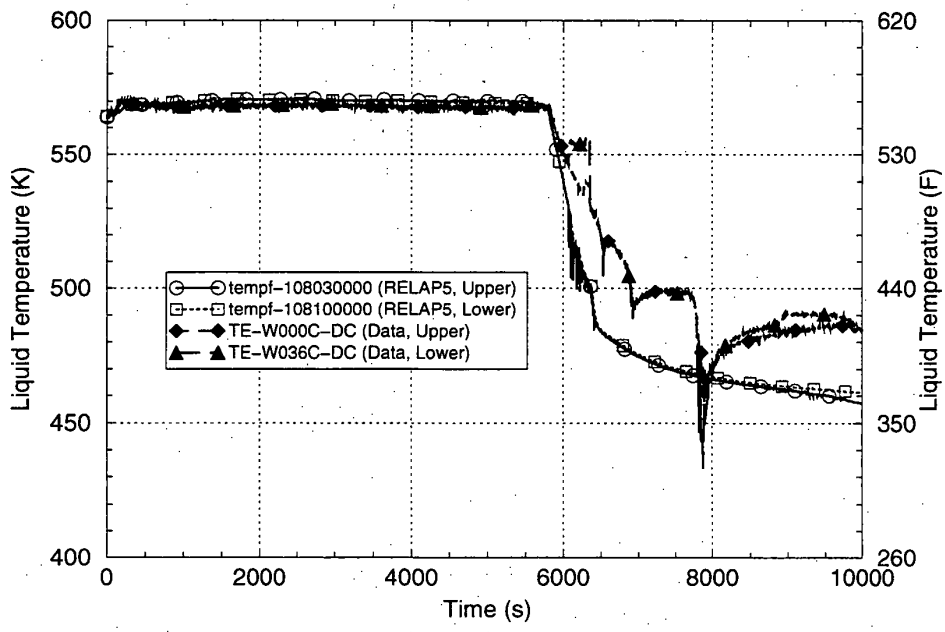

Figure 6.9. Reactor Vessel Downcomer Temperatures (ROSA-IV Test SB-HL-06)

6.7.2.2 ROSA AP-600 Experiments

The ROSA-AP600 facility is a 1/30 volume-scaled, full-pressure representation of a Westinghouse AP600 PWR. The facility utilizes a full-height electrically heated core. The two AP600 coolant loops are represented with two equal-volume loops in the test facility. Components represented in the loops are the hot leg, steam generator, one reactor coolant pump (compared with two pumps in the plant design),

one cold leg (compared with two in the plant design), pressurizer (on one loop), and core makeup tanks (CMTs) on the other loop. The passive residual heat removal (PRHR) system, ADS, and IRWST are also represented in the test facility.

While there are configuration differences between the designs of AP600 and currently operating PWRs, assessments against ROSA/AP600 data are useful for PTS because the cold leg and reactor vessel downcomer regions of the facility are particularly well-instrumented and activation of the ADS effectively causes a transition from a small-break LOCA event sequence to a large-break LOCA event sequence, both of which are of interest for the PTS application. RELAP5 was assessed against two ROSA-AP600 experiments, AP-CL-03 and AP-CL-09.

Test AP-CL-03 represents a 0.1% 1-in. (2.54-cm) diameter scaled break on the bottom of a cold leg in the CMT loop. The reactor is operating at full power when the break opens. An additional failure, where one of the two ADS-4 valves on the CMT loop fails to open, is also assumed.

The comparisons of RELAP5-calculated and measured data for this experiment show that the complex system behavior and timing of the test are well-predicted with RELAP5. The RELAP5 prediction of coolant loop flow stagnation and draining are in good agreement with the test data.

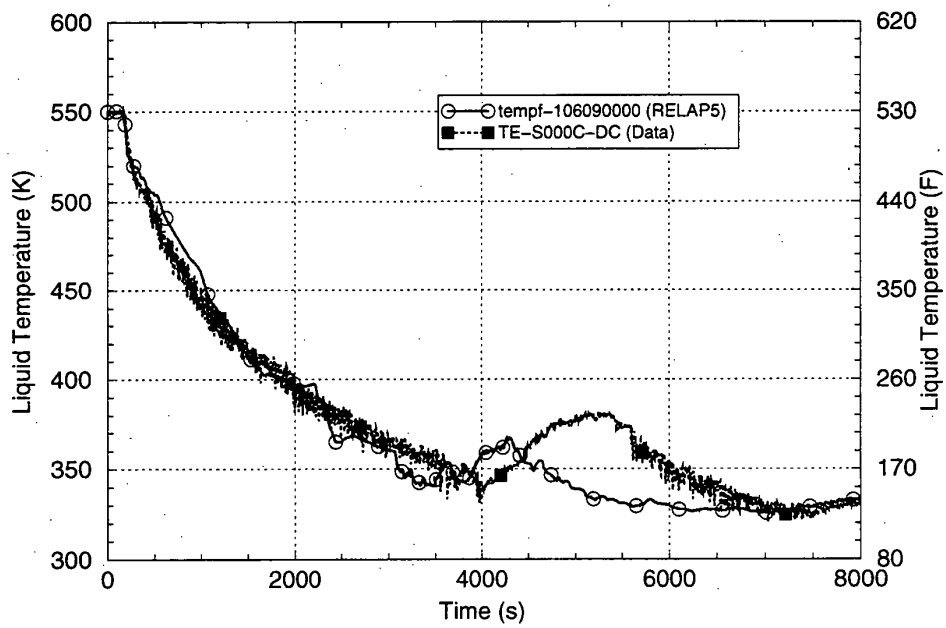

Figure 6.10. Reactor Vessel Downcomer Fluid Temperatures (ROSA/AP600 Test AP-CL-03)

The test exhibits thermal stratification within the cold legs; a layer of cold ECCS water resides under a layer of warmer water within the horizontal cold leg pipes. This thermal-stratification behavior cannot be represented with a one-dimensional computer code such as RELAP5. However, the assessment indicates only minimal effects of this code limitation on the calculated reactor vessel downcomer prediction. Figure 6.10 compares the RELAP5-calculated and measured reactor vessel downcomer fluid temperatures on the pressurizer-loop side of the downcomer at an elevation corresponding to the bottom of the reactor core. The fluid temperature code-data comparisons at other locations in the downcomer are similar. RELAP5 overpredicted the downcomer fluid temperature by a maximum of 59 K (106°F) and underpredicted it by a

maximum of 72 K (130°F). RELAP5 underpredicted the downcomer fluid temperature by an average of 4 K (7°F) over the test period.

Test AP-CL-09 also represents a 0.1% 1-in. (2.54-cm) diameter scaled break on the bottom of a cold leg in the CMT loop. The reactor is operating at full power when the break opens. Although similar to Test AP-CL-03, Test AP-CL-09 represents additional passive safety system failures:

- Both CMT discharge valves fail closed.
- Half of the valves in each ADS stage fail closed.
- ADS (normally activated by low CMT level) activated 30 minutes after a low-low pressurizer pressure signal is generated.
- Check valve in accumulator discharge line on the CMT loop fails closed.
- Check valve in the IRWST discharge line on the CMT loop fails closed.
- Only one-half of the PRHR heat exchanger capability is available.

The comparisons of RELAP5-calculated and measured data for this experiment show that the complex system behavior and timing of the test are well-predicted with RELAP5.

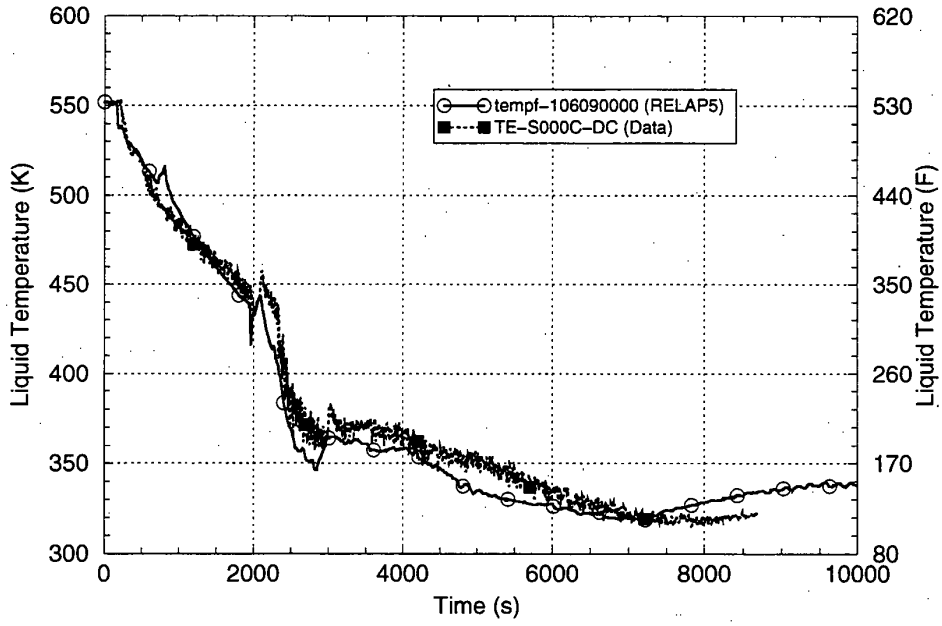

Figure 6.11. Reactor Vessel Downcomer Fluid Temperatures (ROSA/AP600 Test AP-CL-09)

As in Test AP-CL-03, thermal stratification behavior within the horizontal cold legs (which cannot be represented with RELAP5) is observed in Test AP-CL-09. Because of cold leg thermal stratification effects, the sequence order in which two loops stagnated in the RELAP5 calculation was the reverse of that seen in the test. However, good agreement is seen between the calculated and measured first-loop and second-loop stagnation times. The assessment indicates only minimal effects of this code limitation on the prediction of vessel downcomer fluid temperatures. Figure 6.11 compares the RELAP5-calculated and measured reactor vessel downcomer fluid temperatures on the pressurizer-loop side of the downcomer at an elevation corresponding to the bottom of the reactor core. The fluid temperature code-data comparisons at other locations in the downcomer are similar. RELAP5 overpredicted

the downcomer fluid temperature by a maximum of 39 K (71°F) and underpredicted it by a maximum of 49 K (88°F). RELAP5 overpredicted the downcomer fluid temperature by an average of 1 K (2°F) over the test period.

6.7.2.3 APEX Tests

A series of tests specific for plants of Combustion Engineering (CE) design was conducted at the APEX facility operated by Oregon State University. The APEX facility is a ¼-height scale low-pressure integral systems facility that has been configured to model the thermal-hydraulic phenomena of CE plants. The purpose of these tests was to investigate mixing of high-pressure injection fluid in the cold leg and the downcomer and to evaluate the onset of coolant loop flow stagnation, which can lead to low temperatures in the reactor vessel downcomer. Two APEX tests were used for RELAP5 assessment, APEX-CE-13 and APEX-CE-05.

Test APEX-CE-13 represents a stuck-open pressurizer safety relief valve event with the reactor operating at full power. The stuck-open valve is subsequently assumed to reclose. This type of transient event is a significant contributor to PTS risk event because the RCS is first significantly cooled and then repressurized after the relief valve closes. To start the test, the ADS-2 valve atop the pressurizer was opened to simulate a stuck-open pressurizer safety relief valve. Simultaneously, two reactor coolant pumps were tripped, the HPI system was actuated and reactor core power was tripped. The ADS-2 valve was closed at 1 hour into the test and the test was terminated about 20 minutes later after the RCS had refilled.

The comparisons of RELAP5-calculated and measured data from Test APEX-CE-13 indicate that the code is capable of acceptably simulating the behavior of the key PTS parameters for this test. RELAP5 overpredicted the RCS cooldown rate during the period when the relief valve is open as shown in Figure 6.12. RELAP5 predicted a delayed onset of the repressurization and underpredicted the pressurization rate after the relief valve closed as seen in Figure 6.13. These differences between the calculated and measured responses are considered to be moderate and to result from difficulties in adequately modeling the system heat losses of small-scale facilities such as APEX. RELAP5 underpredicted the downcomer fluid temperature by an average of 2 K (4°F) over the test period.

Test APEX-CE-05 was performed to provide baseline mixing data for the injection of cold ECC water into the cold legs of the RCS. During the test, RCS temperatures and pressures consistent with full-power plant operation are first established and then the steam generators, RCPs and reactor core heaters are secured to create stagnant conditions in the RCS. High-pressure injection is initiated into the four cold legs and a pressurizer drain valve is opened to accommodate the injected fluid and control the pressurizer level and RCS pressure. For this test, the behavior of interest is the manner in which the cold water entering the vessel through the cold legs spreads downward and around the reactor vessel downcomer annulus. The thermocouple instrumentation of the facility was upgraded in order to observe this behavior.

The test data exhibit only very small variations in the downcomer temperatures around the periphery of the downcomer. The maximum azimuthal downcomer temperature variations are 9 K (16°F) at the elevation corresponding to the top of the core and are 5 K (9°F) at the elevation corresponding to the bottom of the core. No significant plumes were observed in the downcomer based on the temperature results of this test. Larger variations are seen in the axial direction in the downcomer, but these variations, which are related to the time required for fluid to transit though the downcomer, are short-lived. The downcomer temperature variations observed in the RELAP5 simulation of the test similarly are small.

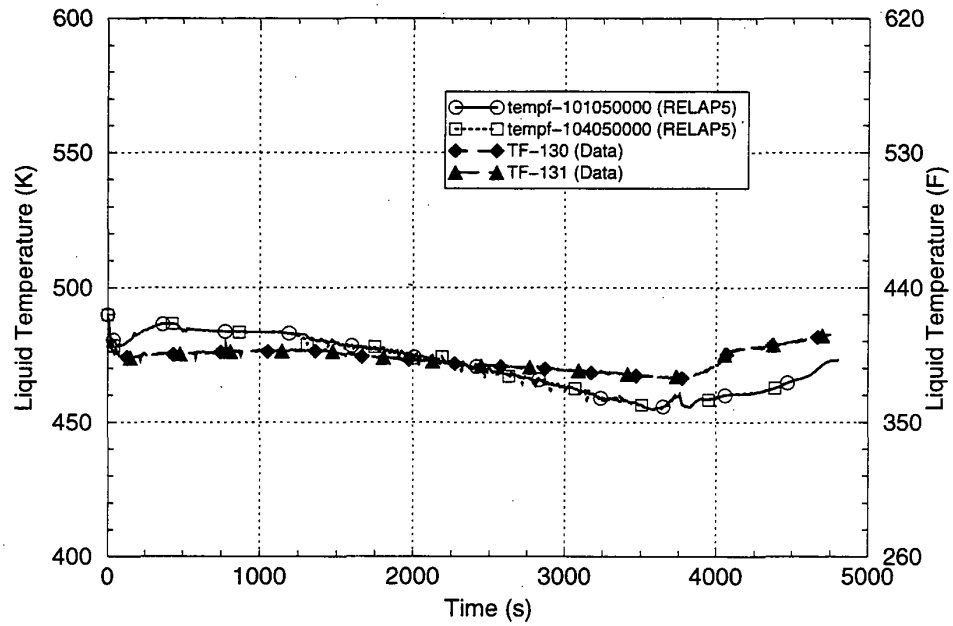

Figure 6.12. Reactor Vessel Downcomer Fluid Temperatures (Test APEX-CE-13)

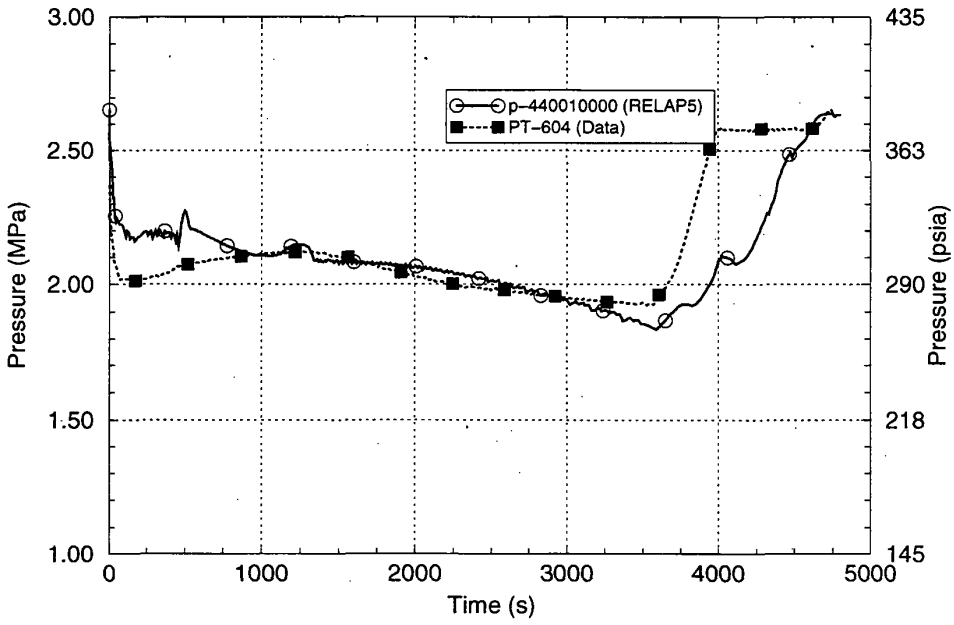

Figure 6.13. Pressurizer Pressure (Test APEX-CE-13)

Figure 6.14 compares the RELAP5-calculated and measured reactor vessel downcomer fluid temperature responses for Test APEX-CE-05 at a representative location (directly under one of the cold legs at an elevation corresponding to the top of the core). The figures show that RELAP5 predicts the downcomer fluid temperature excellently up to about 2,000 s, but then underpredicts it afterward. Over the test period, RELAP5 underpredicted the downcomer fluid

temperature by an average of 5 K (9°F). The underprediction is attributed to more involvement of warm fluid residing within the cold legs in the mixing process in the experiment than in the calculation.

A second sensitivity RELAP5 calculation for Test APEX-CE-05 was performed in which large artificial flow loss coefficients for reverse flow were added in the reactor coolant pump suction regions of each cold leg. This modeling approach is used in PTS plant calculations to suppress circulations through the cold legs on the same coolant loop (in the forward direction through one cold leg and in the reverse direction in the other) for certain types of PTS events. This model change resulted in RELAP5-calculated reactor vessel downcomer fluid temperatures that were additionally lower (compared with the above calculation) by an average of 8 K (14°F) over the test period. This difference represents the expected downcomer temperature conservatism resulting from using the high artificial reverse flow loss coefficient modeling approach.

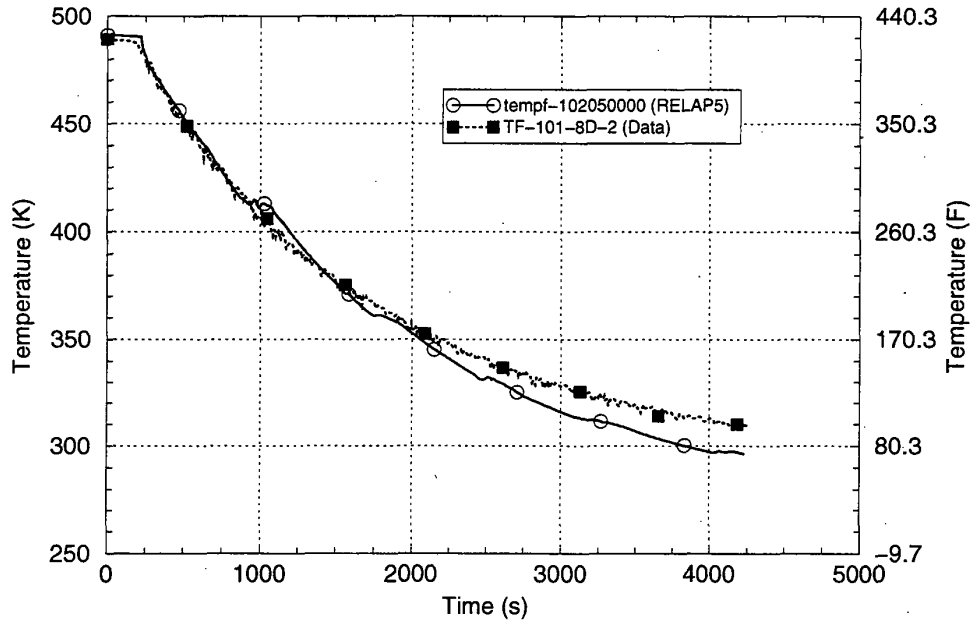

Figure 6.14. Reactor Vessel Downcomer Fluid Temperatures (Test APEX-CE-05)

6.7.2.4 LOFT Tests

The Loss-of-Fluid Test Facility (LOFT) is a 50-MWt volumetrically scaled PWR system. The LOFT facility was designed to obtain data on the performance of the engineered safety features of a commercial PWR system for postulated accidents, including LOCAs.

The LOFT nuclear core is approximately 5.51-ft (1.68-m) tall and 2-ft (0.61-m) in diameter, and is composed of nine fuel assemblies containing 1,300 nuclear fuel rods of representative PWR design. Three intact loops are simulated using a volume/power ratio scaling by the single circulating (intact) loop in the LOFT primary system. The broken loop is simulated by the scaled LOFT blowdown loop.

An ECCS is provided to simulate the engineered safety features in PWRs. An HPI system centrifugal pump and a nitrogen-pressurized accumulator supply emergency core cooling. The LPIsystem and accumulator discharge lines are orificed as required to simulate the delivery characteristics of various PWR emergency core cooling systems.

RELAP5 assessment was performed using three LOFT experiments, Test L3-7, Test L2-5 and Test L3-1.

Loft Test L3-7 represents plant recovery actions following a 1-in. (2.54-cm) equivalent diameter break in the cold leg of a PWR operating at full power. The primary purpose of this test is to establish a break flow approximately equal to the HPI flow at an RCS pressure of approximately 6.9 MPa [1,000 psia], to isolate the break and to demonstrate the stabilization of the plant at cold shutdown conditions.

During Test L3-7, the break was opened, the reactor and reactor coolant pumps were tripped, leading to coolant loop natural circulation flow. At 1,800 s, the AFW and HPI flows were terminated to hasten the loss of RCS fluid inventory and to establish the conditions leading into the system recovery to cold shutdown conditions. At 3,603 s, the AFW flow was reinstated and a SG steam bleed operation begun to effect a controlled depressurization of the intact loop SG secondary system. The HPI flow was reinstated at 5,974 s, and the test was terminated at 7,302 seconds.

The assessment indicates that RELAP5 is capable of acceptably simulating the behavior of the key PTS parameters for LOFT Test L3-7. The RELAP5 prediction of the RCS pressure is in good-to-excellent agreement with the measured data. The RELAP5 prediction of the reactor vessel downcomer fluid temperature is in good agreement with the measured data. Figure 6.15 shows a comparison of the measured and calculated reactor vessel downcomer fluid temperatures for this test at representative locations in the downcomer (on the broken loop and intact loop sides of the downcomer and at elevations in the downcomer corresponding to the elevations of the top and middle of the core). Over the test period, RELAP5 underpredicted the downcomer fluid temperature by an average of 8 K (14°F).

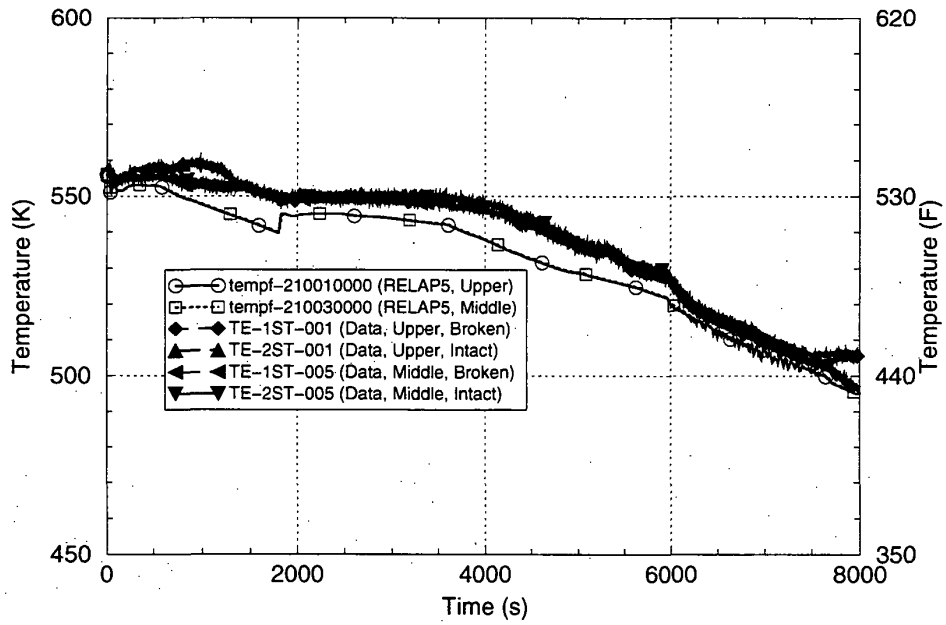

Figure 6.15. Reactor Vessel Downcomer Fluid Temperatures (LOFT Test L3-7)

Test LOFT L2-5 represents a double-ended offset guillotine break LOCA in the cold leg of a PWR operating at full power. The primary purpose of this test was to evaluate the performance of the ECCS for cooling the core. For the purposes of the PTS assessment, this test

provides data for the very rapid blowdown and refilling of the RCS with cold ECCS which accompanies a very large break in the RCS. During the test, the break was opened and the reactor and reactor coolant pumps were tripped. Accumulator injection began when the RCS pressure had declined below the initial accumulator pressure and delayed injection of HPI and LPI ECC coolant began at 24 s and 37 s, respectively after the break opened.

The assessment indicated no major differences between the RELAP5-calculated and measured responses for LOFT Test L2-5. The RELAP5 predictions of the reactor vessel downcomer fluid temperature and RCS pressure are in good agreement with the measured data. Figure 6.16 shows a comparison of the measured and calculated reactor vessel downcomer fluid temperatures for this test at representative locations in the downcomer (on the broken loop side of the downcomer at elevations in the downcomer corresponding to the elevations of the top, middle and bottom of the core). Over the test period, RELAP5 underpredicted the downcomer fluid temperature by an average of 4 K (7°F).

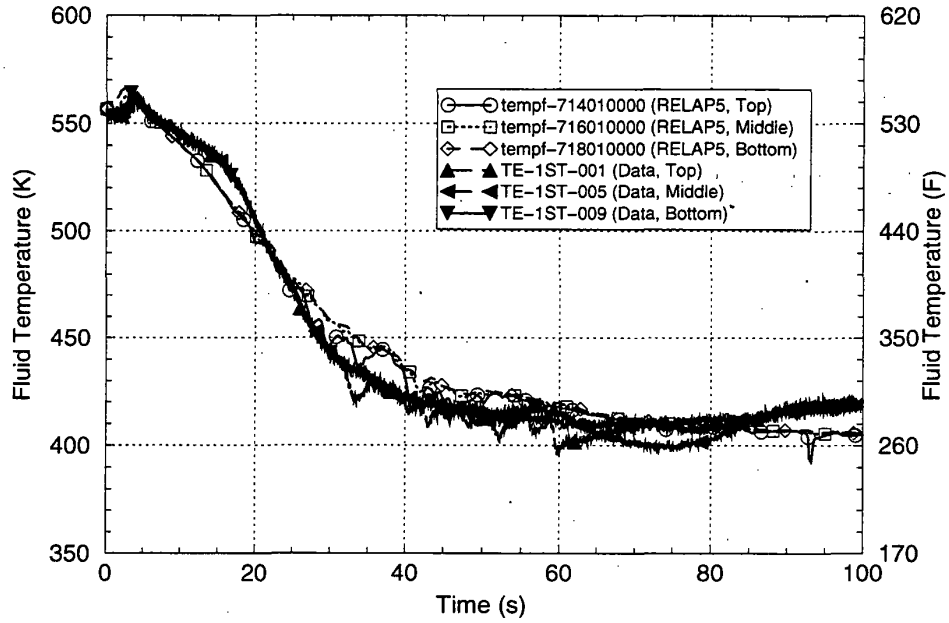

Figure 6.16. Reactor Vessel Downcomer Fluid Temperatures (LOFT Test L2-5)

LOFT Test L3-1 represents an equivalent 4-in. (10.16-cm) diameter break LOCA in the cold leg of a PWR operating at full power. The primary purpose of this experiment was to evaluate the performance of the ECCS for cooling the core.

During the experiment, the reactor and the reactor coolant pumps were tripped and ECC flows from the HPI and accumulator systems were initiated as the RCS pressure declined. The accumulator water inventory was fully discharged and the experiment was continued until 3,623 s using the HPI ECC flow alone. At that time a feed-and-bleed SG cooling process was implemented; the experiment was concluded at 4,368 s.

For the purposes of the PTS assessment, this test provides data for the rapid blowdown and stabilization of the RCS with ECCS injection for a break diameter that is toward the larger end of the small-break LOCA spectrum.

Test L3-1 also provides data useful for comparing RELAP5 simulation capabilities when using one-dimensional and two-

dimensional reactor vessel downcomer modeling approaches. RELAP5 PTS plant simulations have shown considerable variation in calculated downcomer temperatures for cold leg LOCAs with break diameters near 4-in. (10.2-cm), depending upon whether the 1-dimensional or 2-dimensional RELAP5 downcomer modeling approach is used. RELAP5 calculations for LOFT Test L3-1 are performed using both downcomer modeling approaches in order to judge which approach is better for simulating cold leg breaks of this approximate size.

The assessment indicated that the behavior in the reactor vessel downcomer region is particularly difficult to predict for a break of this size and location. Accumulator injection has a potential for directly influencing the downcomer temperature, but mixing within the cold leg and upper downcomer regions significantly affects that influence. The prediction of mixing within the thermally stratified cold leg regions is beyond the capability of RELAP5. The break is large enough that the RCS depressurizes sufficiently to result in accumulator injection, but not so large as to allow for an accumulator discharge that is insensitive to the RCS pressure. Finally, the break location in the cold leg adds to the prediction difficulty because the most direct path for steam to reach the break is upward through the downcomer, against the downward flow of cold accumulator water. Therefore, interphase condensation modeling, known to be a weakness of RELAP5, appears to be particularly important for predicting the behavior for this particular break size and location

The assessment indicates that RELAP5 is capable of acceptably predicting the reactor coolant system parameters for this test. The downcomer fluid temperatures in the test were underpredicted using both the 1- and 2-dimensional downcomer modeling approaches. Over the test period, the underprediction is by an average of 7 K (13°F) when using the one-dimensional downcomer modeling scheme and by an average of 13 K (23°F) when using the 2-dimensional downcomer modeling scheme. Figure 6.17 compares the measured and calculated fluid temperatures for Test LOFT L3-1 at a representative location in the reactor vessel downcomer. The data shown are for a location on the broken loop side of the downcomer at an elevation corresponding to the middle of the reactor core. The code-data comparisons at other locations in the downcomer are similar.

The 2-dimensional reactor vessel downcomer modeling approach is judged to be the more appropriate approach for RELAP5 PTS applications because of (1) the better accumulator injection behavior it produced, (2) the ability it provides for predicting different fluid behavior in the intact and broken-loop sides of the reactor vessel downcomer, which has the potential to affect break flow and downcomer mixing, and (3) the more conservative downcomer fluid temperature predictions it produced.

More detailed information regarding the assessment of RELAP5 for LOFT Test L3-1 is found in Section 3.9 of [***Fletcher***].

6.7.2.5 MIST Tests

The Multi-loop Integral System Test (MIST) facility is a scaled full-pressure experimental facility that represents the B&W lowered-loop plant design with two hot legs and four cold legs. The plant-to-facility power scaling factor is 817, and the plant-to-facility volume scaling factor is 620 for the total primary system volume, excluding the core flood tanks. Major components include two once-through steam generators with full length tubes, two hot leg pipe segments, four cold leg pipe segments, four coolant pumps, a reactor vessel with an external downcomer, a pressurizer with spray and PORV connections, and one core flood tank. Boundary systems provide simulation of the HPI, auxiliary feedwater, and various types of failures such as steam generator tube ruptures and LOCAs.

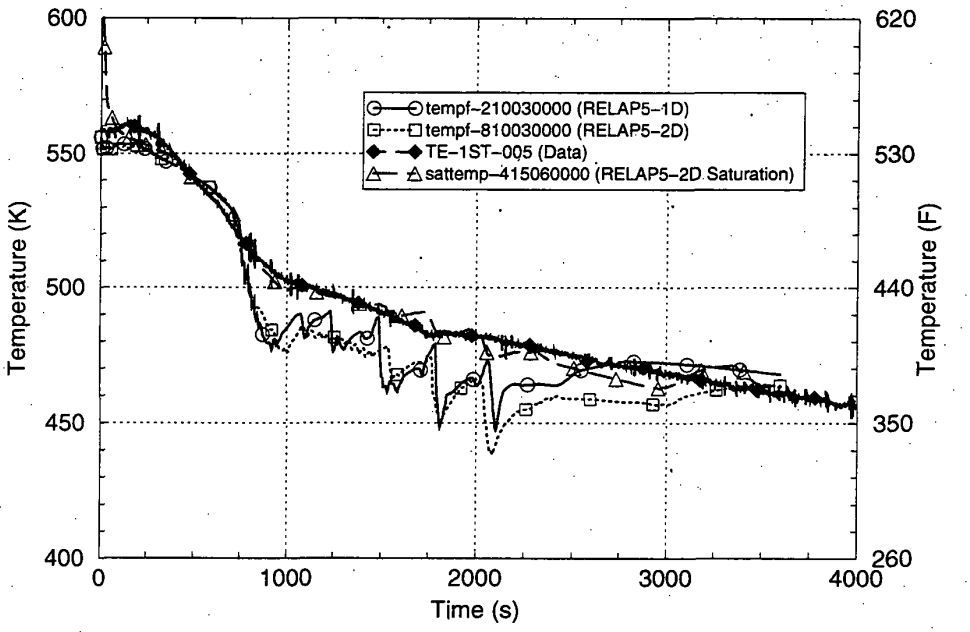

Figure 6.17. Reactor Vessel Downcomer Fluid Temperatures (LOFT Test L3-1)

RELAP5 assessment was performed for three MIST experiments, Test 360499, Test 3109AA, and Test 4100B2.

MIST Test 360499 is a HPI-power operated relief valve (HPI-PORV) feed-and-bleed simulation, starting from 110% flow, 10% scaled-power conditions. The system behavior for this test resembles a stuck-open pressurizer PORV event sequence with continued HPI injection and operator throttling based upon the RCS subcooling margin. Events such as this are significant contributors to the risk of PTS vessel failure.

The assessment for this test indicated that the RELAP5 prediction of the RCS pressure was excellent. However, the assessment indicated major differences between the calculated and measured responses within the cold legs on the two coolant loops. RELAP5 overpredicted the cold leg temperature in Loop A, and did not predict the coolant loop flow stagnation seen in the test. RELAP5 underpredicted the cold leg temperature in Loop B and did predict the coolant loop flow stagnation seen in the test.

Despite these difficulties, the RELAP5 prediction of the reactor vessel downcomer fluid temperature, which represents a mixture of the cold leg temperatures, was judged to be good. Figure 6.18 compares the calculated and measured reactor vessel downcomer fluid temperatures for MIST Test 360499 at a representative location in the downcomer (at an elevation corresponding to the bottom of the core). The code-data comparisons at other downcomer locations are similar. Over the test period, RELAP5 overpredicted the downcomer fluid temperature by an average of 3 K (5°F).

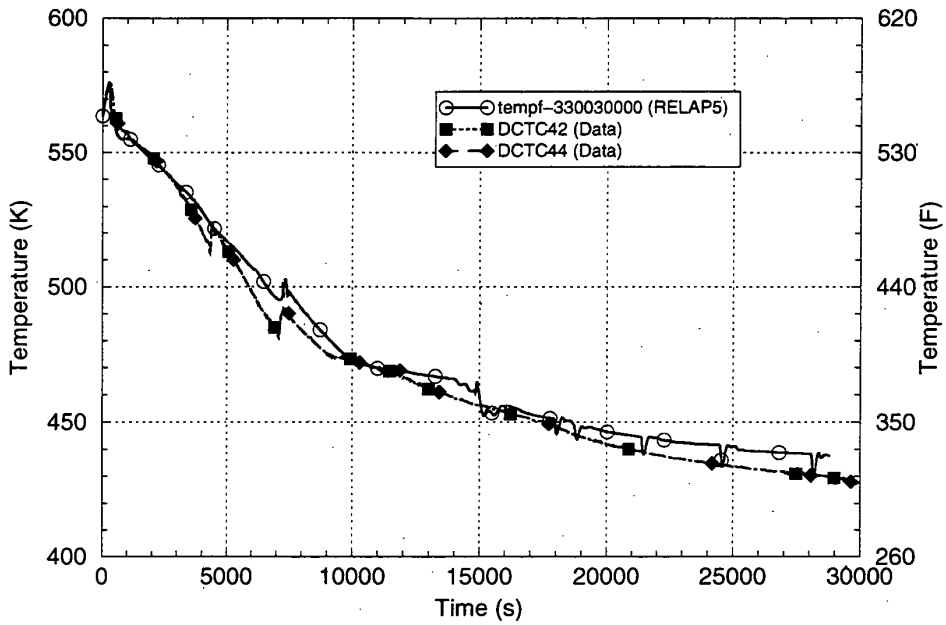

Figure 6.18. Reactor Vessel Downcomer Fluid Temperatures (MIST Test 360499)

MIST Test 3109AA represents a 1.6-in.^{2} (10-cm^2) break in the RCP discharge section of a PWR cold leg. This break size corresponds to a 1.4-in. (3.59-cm) diameter break in the PWR and is sufficiently small that HPI flow can compensate for break flow. At the start of the test, the facility is operating under natural-circulation loop flow conditions, with the RCP rotors locked.

The assessment indicated no major differences between the calculated and measured data for MIST Test 3109AA. The RELAP5 prediction of the RCS pressure is in good agreement with the measured data. The code well-predicted the interruption of loop natural circulation flow in both of the coolant loops. RELAP5 overpredicted the reactor vessel downcomer fluid temperature after about 1,000 s. Figure 6.19 compares the calculated and measured reactor vessel downcomer fluid temperatures for MIST Test 3109AA at a representative location in the downcomer (at an elevation corresponding to the top of the core). The code-data comparisons at other downcomer locations are similar. Over the test period, RELAP5 overpredicted the downcomer fluid temperature by an average of 10 K (18°F).

MIST Test 4100B2 represents a 15.5-in.^{2} (100-cm^2) [4.4-in. (11.2-cm) diameter] equivalent break in the RCP discharge section of a PWR cold leg. The break size is sufficiently large that HPI cannot compensate for the break flow. The test is initiated at conditions representing 3.5% scaled power and coolant loop natural circulation conditions with the RCPs tripped and their rotors locked. During the test, the core power is tripped and HPI and EFW flows are initiated.

The assessment for MIST Test 4100B2 shows moderate differences between the calculated and measured data for the most important parameters for PTS (RCS pressure and downcomer fluid temperature). Following the RCS blowdown, basic limitations of RELAP5 resulted in an underprediction of the stable RCS pressure by about 0.68 MPa [98 psi]. RELAP5 slightly underpredicted the downcomer fluid temperatures during the blowdown period, up to about 2,100 s. However, during the refill period RELAP5 overpredicted the reactor vessel

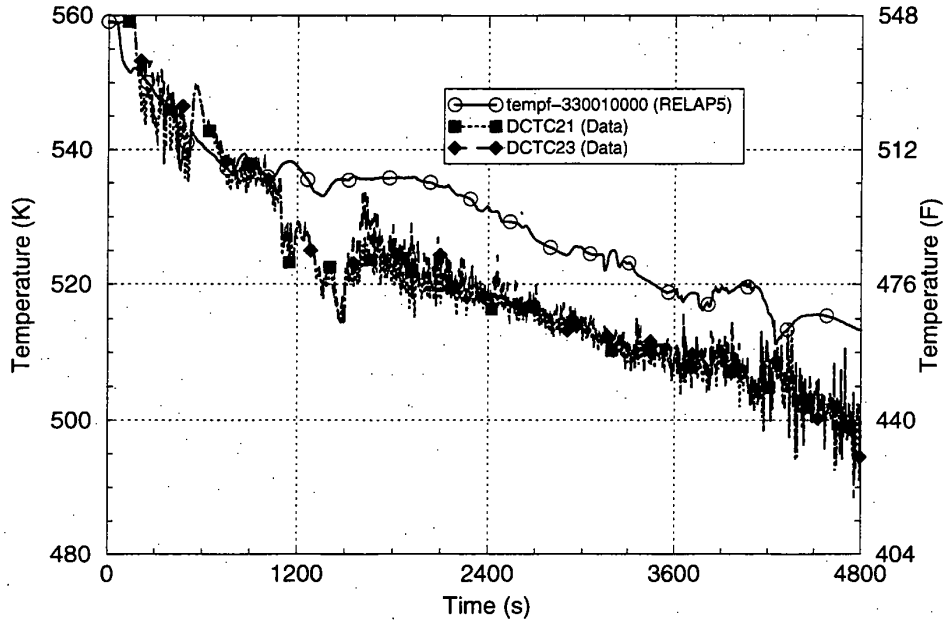

Figure 6.19. Reactor Vessel Downcomer Fluid Temperatures (MIST Test 3109AA)

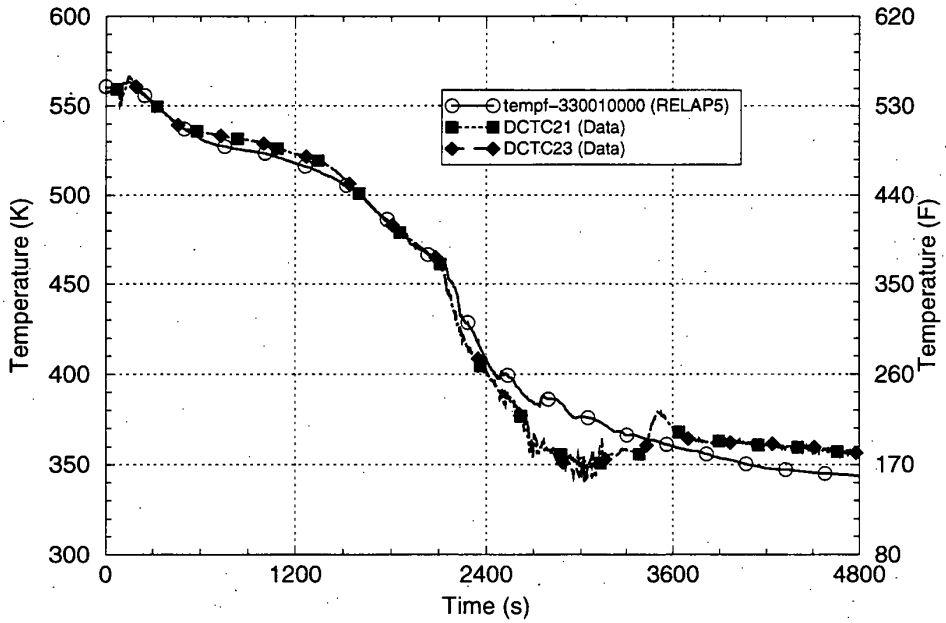

Figure 6.20. Reactor Vessel Downcomer Fluid Temperatures (MIST Test 4100B2)

downcomer fluid temperature by up to 32 K (58 °F). Figure 6.20 compares the calculated and measured reactor vessel downcomer fluid temperatures for MIST Test 4100B2 at a representative location in the downcomer (at an elevation corresponding to the top of the core). The code-data comparisons at other downcomer locations are similar. Over the test period,

RELAP5 overpredicted the downcomer fluid temperature by an average of 0.37 K (0.67°F).

6.7.2.6 Reactor Vessel Wall Inside-Surface Heat Transfer Coefficient

For the reactor vessel wall heat transfer coefficient, quantitative assessment comparisons are more difficult than for RCS pressures and downcomer fluid temperatures because heat transfer coefficients are not directly measured in the experiments. Further, since most of the test facilities were designed to study core-coolability safety issues and not vessel downcomer overcooling issues, experimental instrumentation related to downcomer wall heat transfer (wall and fluid thermocouples, wall heat fluxes and downcomer fluid velocities) is generally limited. Quantitative assessments of RELAP5 capabilities for predicting the vessel wall heat transfer coefficient and other heat transfer-related parameters are provided in this section to the extent feasible considering the limited available data. Other investigations into reactor vessel wall heat transfer in general and RELAP5 capabilities in particular are also presented here to support the assessment conclusions regarding the wall heat transfer coefficient. The information in this section summarizes that presented in greater detail elsewhere [***Bessette***].

As described below, for the PTS application, the wall heat transfer regime of greatest interest is for wall-to-fluid convection for Reynolds numbers toward the low end of the turbulent range. This regime corresponds to the reactor vessel downcomer situation during periods with low coolant-loop natural circulation flow or periods after the coolant-loop flows have stagnated as a result of voiding in the upper regions of the RCS (as is caused by draining during LOCA events). Other heat transfer regimes are also experienced during portions of the PTS transient accident scenarios. Highly turbulent forced convection is experienced when reactor coolant pumps are operating or when there is robust coolant-loop natural circulation flow. Saturated and subcooled nucleate boiling are generally experienced for events where the RCS rapidly depressurized, the fluid saturation temperature quickly drops and the hot vessel wall passes heat to a flashing and boiling fluid. The attention is given here to the regime for convection because it (1) is frequently encountered in the PTS scenarios, and (2) results in a relatively low heat transfer coefficient. The other regimes (highly turbulent convection and boiling) result in large heat transfer coefficients. A detailed assessment of the accuracy of RELAP's heat transfer models is not warranted in these other regimes because the process of wall-to-fluid heat transfer is dominated by the surface boiling transport mechanism and not by the convective movement of fluid. Therefore, the heat transfer is less influenced by details of bulk fluid motion

6.7.2.6.1 Effect of Heat Transfer Coefficient on Wall Heat Flux

During normal steady plant operation, the reactor vessel wall temperature is the same as the downcomer fluid temperature (which is core inlet temperature). During PTS scenarios, the fluid temperature falls. The wall-to-fluid heat transfer processes from the hotter vessel wall to the colder fluid in the downcomer are of significance. The RCS cooldowns experienced in the PTS accident scenarios generally fall into three categories of (1) secondary-side events, such as main steam line breaks, (2) small primary-side LOCAs, such as hot or cold leg breaks or stuck-open pressurizer relief valve events, and (3) large primary-side LOCAs, such as double-ended hot or cold leg breaks. Each of these event categories is separately discussed in the following subsections.

6.7.2.6.1.1 Secondary Side Events

For secondary-side events, the RCS is rapidly cooled by overcooling to the steam generators but the RCS remains at high pressure and, often, forced flow of coolant through the RCS loops continues. The RCS fluid cools, but the extent of the cooldown is limited because the ultimate heat sink temperature is the saturation

temperature at atmospheric pressure, which represents the final state in the secondary coolant system. The reactor vessel wall heat transfer coefficient remains high as a result of pump-forced flow or a robust coolant-loop natural circulation flow for cases where the reactor coolant pumps are tripped. As a result, the wall-to-fluid heat transfer process is controlled by heat conduction through the reactor vessel wall.

6.7.2.6.1.2 Small Primary Side LOCAs

For small primary-side LOCA events, the RCS depressurizes at a rate that is proportional to the break size. Fluid flashing caused by the RCS depressurization cools the RCS fluid as the saturation temperature falls. The ECC systems add cold water to the RCS at rates that increase with decreasing RCS pressure. This pressure dependency results because the ECC systems are made up of (1) tanks (accumulators, core flood tanks, and safety injection tanks) with cold water inventory stored at intermediate pressures, and (2) centrifugal pump systems (HPI, LPI, etc.) for which no flow is delivered above the pump shutoff heads and for which lower RCS pressures lead to greater cold water injection flow rates.

For the small LOCAs, the system pressure is defined by the RCS mass and energy balances associated with core heat addition, cold water injection, steam generator heat removal, and break flow. There is much interdependence among the PTS parameters of interest (pressure, fluid temperature, and heat transfer coefficient).

Larger break sizes lead to lower pressures (which tend to mitigate the PTS risk) while at the same time leading to higher ECC injection rates and lower fluid temperatures (which tend to increase the PTS risk). Further, the variations in the injection flow rate can directly affect the break flow (which, in turn, affects RCS pressure) and the RCS inventory, which affects tripping of reactor coolant pumps, coolant loop natural circulation and stagnation, vessel downcomer velocities and wall heat transfer coefficients. For small primary-side LOCA events, the potential for vessel failure as a consequence of PTS arises as a result of incomplete RCS depressurization and RCS draining, which causes the stagnation of the coolant-loop natural circulation flows and leads to pooling of cold water in the cold leg and downcomer regions.

Because for small breaks, the injection of cold ECC water is at a low rate, the RCS cooldown experienced for this category of LOCA events is relatively slow and there is a feedback between the heat transfer from the wall to the fluid and the fluid temperature itself. For this category of events, the downcomer wall heat transfer regimes generally fall into the range of turbulent forced convection from wall to subcooled liquid (even following coolant loop flow stagnation, the downcomer flow rates remain sufficiently high to resemble forced convection).

6.7.2.6.1.3 Large Primary Side LOCAs

For large primary-side LOCA events, the RCS completely depressurizes and the injections of cold ECC water from the HPI, LPI, and accumulator systems are at very high rates. The rapid decline in the fluid saturation temperature leads to limited periods of fluid flashing and boiling on the hot vessel wall. Heat transfer coefficients are very high for conditions of nucleate boiling. As a result of the large break size, the RCS cannot repressurize from the ECC injection. The high injection rate floods the cold legs and vessel downcomer regions with cold water and this quickly terminates the boiling process.

6.7.2.6.2 Comparison of Measured and RELAP5-Calculated Reactor Vessel Wall Heat Transfer Data

Only limited pertinent data are available from integral system tests for assessing RELAP5 reactor vessel wall-to-fluid heat transfer for geometries consistent with the plants and the conditions present in the PTS accident scenarios. Instruments are often not available for directly measuring heat transfer coefficient or heat flux. However, downcomer fluid and vessel wall

thermocouple data along with fluid velocity data are occasionally available that permit a quantified comparison between the measured and RELAP5-calculated wall heat transfer process. This section summarizes vessel wall-to-fluid heat transfer comparisons pertinent for the PTS for tests performed in the UPTF, APEX-CE, and Creare test facilities.

6.7.2.6.2.1 UPTF Test 1 Run 21

The UPTF featured a full-scale representation of the reactor vessel, downcomer, and cold legs of a PWR. Test 1 Run 21 consisted of injecting cold HPI water into one of the four cold legs (Cold Leg 2) into a system that was initially filled with hot pressurized water. The experimental conditions are comparable to those experienced in a PWR following stagnation of the coolant loop natural circulation flow. This experimental facility and test were modeled with RELAP5 and the calculated results were compared with the measured test data. The RELAP5 model included a 2-dimensional nodalization scheme, comparable to those employed in the PTS plant analyses.

The measured velocity data at the core-bottom elevation in the downcomer exhibited a downward flow below Cold Leg 2 and upward flows through other azimuthal sectors of the downcomer as shown in Figure 6.21. (The direction of positive velocity is downward.) The RELAP5 simulation also showed a downward water flow below Cold Leg 2 (Figure 6.22), but with the cold water spreading into sectors adjacent to Cold Leg 2 by the time the flow reached the core bottom elevation. As a result, the RELAP5-calculated velocities are seen in these figures to be lower than the measured velocities. The fluid velocities in the downcomer (in both the test and calculation) were much greater than the superficial fluid velocity based on only the HPI flow in the downcomer. The test data indicated that the downcomer velocity is ~16 times the downcomer HPI superficial velocity.

An assessment of the RELAP5-calculated vessel wall heat transfer coefficient was made using fluid and wall thermocouple data. In downcomer regions away from Cold Leg 2, RELAP5 was found to underpredict the rates of decline in both the fluid and vessel wall temperatures by a similar extent and therefore to predict the heat transfer coefficient well (within ~15%). Below Cold Leg 2, RELAP5 was found to underpredict the wall-to-fluid differential temperature of the test as shown in Figure 6.23 and to also underpredict the wall-to-fluid heat flux (as indicated by the slower cooldown rate at the location of a thermocouple embedded 1-in. (25-mm) into the vessel wall at the core top elevation; see Figure 6.24). Since the RELAP5 underprediction of the differential temperature was much greater than the RELAP5 underprediction of the heat flux, RELAP5 was found to overpredict the wall-to-fluid heat transfer coefficient under Cold Leg 2 for UPTF Test 1-21 by a factor of ~2.

6.7.2.6.2.2 APEX-CE Test 5

The Advanced Plant Experiment facility (APEX-CE) is a reduced-height, pressure, and temperature facility scaled to Palisades, a CE-designed plant. The test consisted of injecting cold HPI water into all four cold legs of a system that was initially filled with hot pressurized water. The experimental conditions are comparable to those experienced in a pressurized water reactor following stagnation of the coolant loop natural circulation flow. This experimental facility and test were modeled with RELAP5 and the calculated results were compared with the measured test data. The RELAP5 model included a two-dimensional nodalization scheme, comparable to those employed in the PTS plant analyses.

The RELAP5 assessment concentrated on the first 1,700 s of the test period. There was excellent agreement between measured and calculated fluid and wall temperatures as shown in Figure 6.25 and Figure 6.26. The excellent match between the measured and calculated wall temperatures indicated that RELAP5 also predicts the wall heat flux well. However, a comparison between the measured and calculated wall-to-fluid differential temperatures indicated that RELAP5 underpredicted the test differential temperature by a factor of ~2 and,

therefore, overpredicted the wall-to-fluid heat transfer coefficient for APEX-CE-5 by the same factor.

There are no direct measurements for downcomer flow velocity in the APEX-CE facility, but flow velocity indications were derived from thermocouple data. The calculations indicated that the RELAP5 and measured flow velocities are in good agreement and that (after scaling up for a full-height downcomer) the data indicate that the downcomer circulating flow velocity is a factor of ~20 greater than the superficial velocity of the HPI flowing alone in the downcomer region.

6.7.2.6.2.3 Creare Fluid Mixing Tests

Creare performed experiments in a one-half linear scale facility to investigate fluid mixing in a downcomer region for a stagnant coolant-loop situation. The facility represents the region of a single cold leg and one-fourth of the reactor vessel downcomer. The downcomer configuration included a thermal shield installed in the center of the downcomer span. Two NRC tests, MAY105 and MAY106 were performed to simulate cold water injection into an initially hot downcomer (RELAP5 simulations for these tests were not performed). Velocity measurements for two tests indicated velocity ratios (downcomer velocity to superficial downcomer velocity based on HPI flow) of 21 and 26. The downcomer flow was found to contain regions of up-flow and down-flow, with the down-flow velocities greater than the up-flow velocities. The downcomer flow pattern was found to be buoyancy induced.

Figure 6.27 shows that the heat transfer data for the Creare tests are proportional to the Dittus-Boelter correlation. An enhancement of the heat transfer by a factor of ~1.55 above the Dittus-Boelter correlation is seen in the figure for down flow regions but not elsewhere. The enhancement is attributed to entrance effects to which the thermal shield configuration may contribute. In modeling convective heat transfer, RELAP5 applies the maximum of Churchill-Chu for free convection and Dittus-Boelter for forced convection. At low flow velocities (e.g., < ~1 m/s), Churchill-Chu provides higher heat transfer coefficients than Dittus-Boelter.

6.7.2.6.2.4 Summary and Discussion

Three sets of experiments related to injection of cold water into stagnant initially hot water in the reactor vessel downcomer region of a pressurized water reactor have been described in this section. The situation represented by these tests is consistent with that following coolant-loop stagnation in many of the PTS accident scenario categories. The experiments all indicate that the buoyancy effects of cold water entering the downcomer through the cold legs set up a circulation within the downcomer region. The downcomer circulation velocities are seen to be larger than the superficial velocity (that which would result in the downcomer from the ECC injection flow alone) by factors of ~16 to 26.

In the UPTF and APEX-CE assessments, RELAP5 with a two-dimensional downcomer nodalization is seen to be able to capture on a first-order basis the flow pattern and velocities in the downcomer region. Based on comparison between measured and RELAP5-calculated wall and fluid temperature data, RELAP5 is seen to provide reasonable representations of the vessel wall inside surface heat transfer coefficient. For the UPTF test, RELAP5 is seen to provide a good representation (within ~15%) of the heat transfer coefficient for downcomer regions away from Cold Leg 2 (the only cold leg through which the cold water enters the vessel) and to overpredict the heat transfer coefficient by a factor of ~2 for the region under Cold Leg 2. For the APEX-CE test (for which cold water enters the vessel through all cold legs), RELAP5 is seen to overpredict the heat transfer coefficient for all downcomer regions, again by a factor of ~2. Creare data corroborate UPTF and APEX-CE data in showing enhanced large eddy circulating flows in the downcomer. The relatively high velocities result in good heat transfer as seen in the data and predicted by RELAP5. The integrated assessment of RELAP5 for downcomer heat transfer shows the

predictions of the RELAP code to be either realistic or conservative.

6.7.2.6.3 Comparison of RELAP5-Calculated and CFD-Calculated Downcomer Flows

A comparison was made between RELAP5 and COMMIX CFD code solutions for the flow patterns experienced in the reactor vessel downcomer. The comparison was made during the coolant-loop flow stagnation period following a 2-inch (5.1-cm) hot-side break accident scenario in a three-loop Westinghouse plant.

The comparison indicated that RELAP5 adequately captured the overall flow patterns but not finer-scale eddy-flow behavior seen in the COMMIX run. The flow velocities from the COMMIX and RELAP5 calculations were similar and on the order of 19.7 to 39.4 in/s (0.5 to 1.0 m/s).

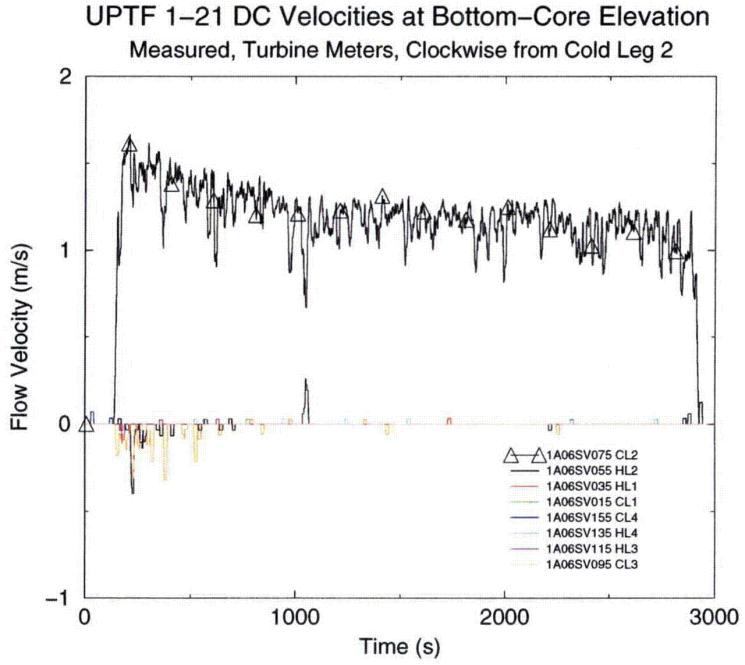

Figure 6.21. UPTF 1-21 DC Velocities at Bottom-Core Elevation Measured, Turbine Meters, Clockwise from Cold Leg 2, Filtered

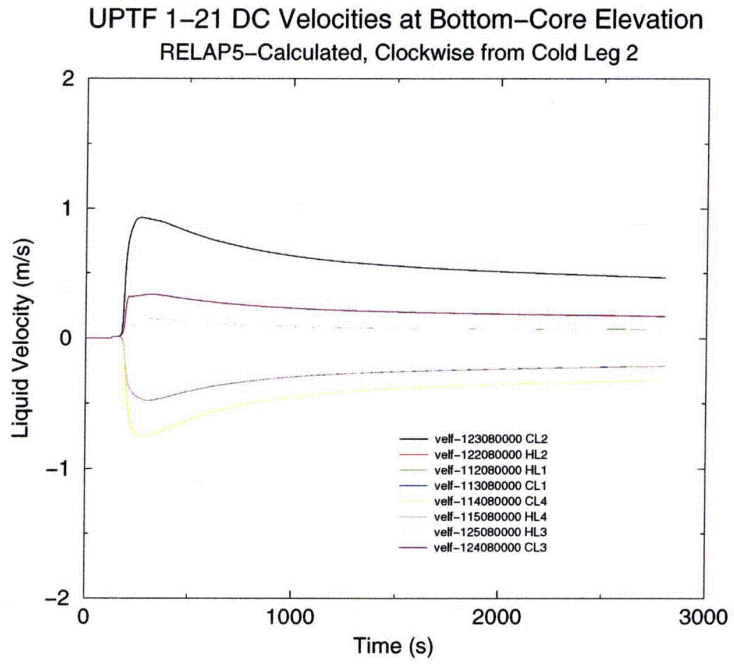

Figure 6.22. UPTF 1-21 DC Velocities at Bottom-Core Elevation RELAP5 (Calculated, Clockwise from Cold Leg 2)

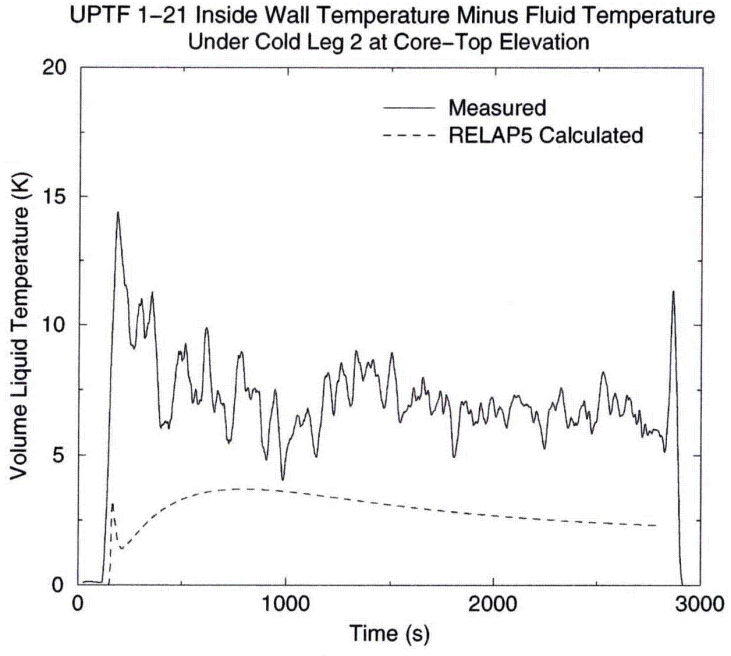

Figure 6.23. UPTF 1-21 Wall Temperature Minus Fluid Temperature Under Cold Leg 2 at Core-Top Elevation

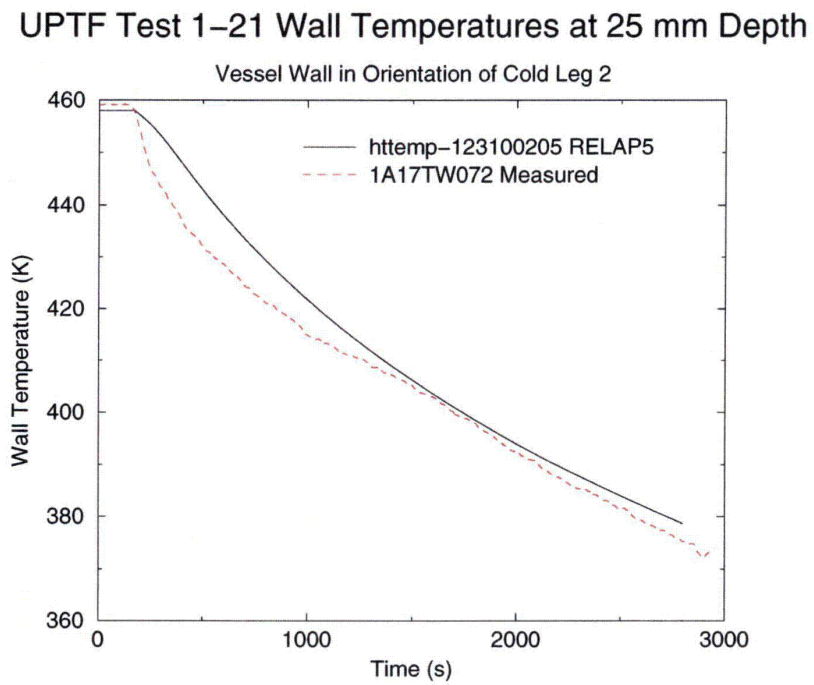

Figure 6.24. UPTF Test 1-21 Wall Temperatures at 25 mm Depth Vessel Wall in Orientation of Cold Leg 2

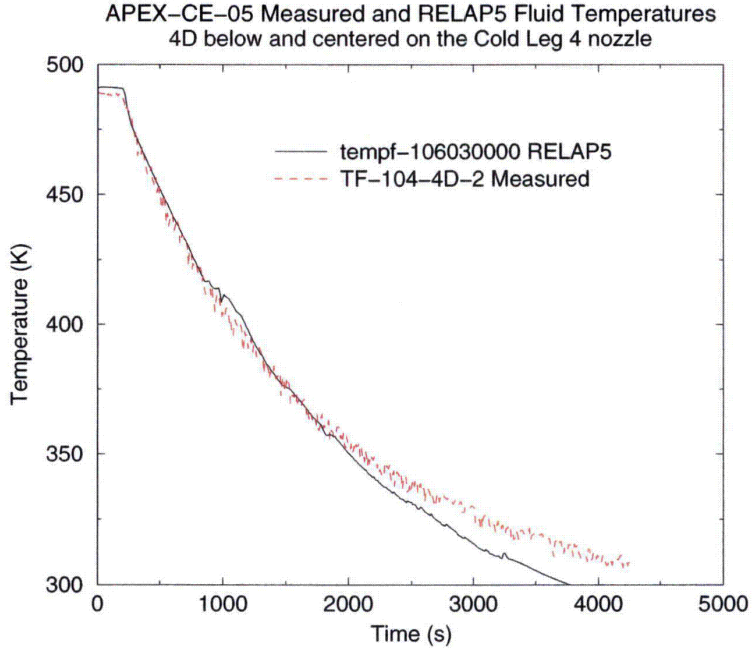

Figure 6.25. APEX–CE–05 Measured and RELAP5 Fluid Temperatures 4D below and centered on the Cold Leg 4 nozzle

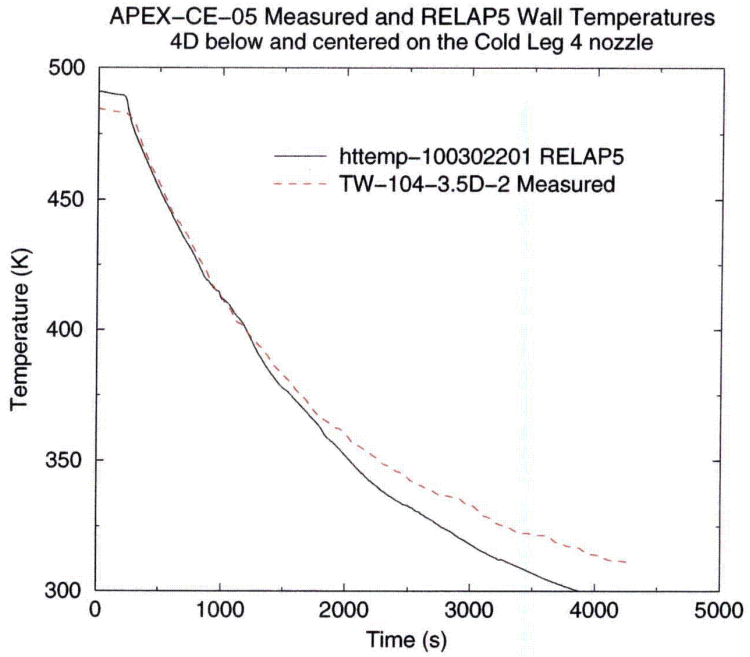

Figure 6.26. APEX–CE–05 Measured and RELAP5 Wall Temperatures 4D below and centered on the Cold Leg 4 nozzle

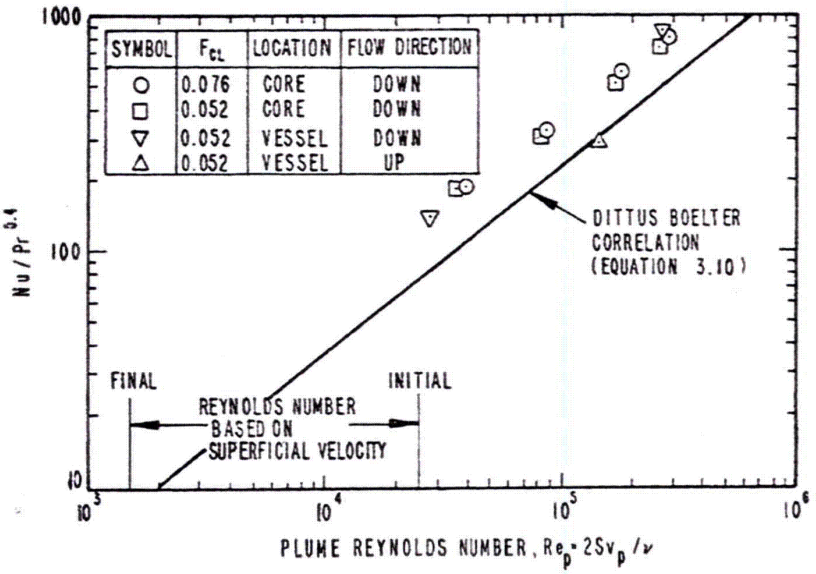

Figure 6.27. Creare Data Compared to Dittus-Boelter

6.7.3 RELAP5 Assessment Conclusions

An assessment has been performed of the RELAP5/MOD3.2.2Gamma computer code capabilities for predicting the parameters of importance for evaluating PTS risk during PWR plant accident scenarios, focusing on the RCS pressure and the temperature of the fluid in the reactor vessel downcomer region. The assessment is performed by comparing the results from RELAP5 simulations of pertinent separate-effects and integral-effects tests with measured test data for experiments in facilities scaled to PWRs. Qualitative judgments are made regarding the overall fidelity of the RELAP5 test predictions. Quantitative estimates also are made of the average uncertainties in the RELAP5 predictions for the important PTS parameters.

The RELAP5 PTS assessment uses data from six experiments in four different separate-effects experimental facilities and from eleven experiments in five different integral-effects experimental facilities.

The separate-effects experiments specifically address (1) pressurizer draining and filling; (2) critical break flow; (3) steam and water behavior in the reactor vessel lower plenum and downcomer regions during the end-of-blowdown and refill periods of LBLOCAs; and (4) single-phase, two-phase, and reflux cooling mode loop natural circulation phenomena under primary-side and secondary-side degraded inventory conditions. These represent phenomena that are significant for the prediction of the important PTS parameters.

The results of the 18 assessment cases generally indicated good and excellent agreement between the RELAP5 calculations and the measured test data. The conclusion from the RELAP5/MOD3.2.2Gamma PTS assessment is that the code is capable of well-predicting the phenomena of importance for evaluating PTS risk in PWRs. The average uncertainty in the RCS pressure prediction is characterized as ±0.2 MPa (±29 psi). The average uncertainty in the reactor vessel downcomer fluid temperature prediction is characterized as ±10 K (±18°F).

6.8 Sensitivity and Uncertainty Analysis

Sensitivity studies were performed to evaluate the effect of key parameters on the RELAP5 prediction of downcomer conditions. These sensitivity studies formed the basis for the assessment of uncertainty in the thermal-hydraulic analysis. The purpose of the uncertainty analysis was to provide adjustments to PRA bin probabilities based on key thermal-hydraulic parameters that significantly affect downcomer conditions, principally temperature.

6.8.1 Sensitivity Analysis

Table 6.2 presents a summary of the results of the sensitivity studies performed as part of the thermal-hydraulic analysis. Many of these sensitivity studies were used to guide the definition of the transients analyzed in this study and to guide the uncertainty assessment discussed later in this section. In addition to the sensitivity studies listed in Table 6.2, evaluations were performed on convective heat transfer from the reactor vessel to the downcomer fluid and on the effect of the in-vessel circulation flows on downcomer conditions.

The heat transfer coefficient model for mixed convection used in RELAP5/MOD3.2.2Gamma is computed as the maximum of the forced convection, laminar convection, and natural convection values. The correlations used are by Dittus-Boelter, Kays, and Churchill-Chu. However, the flow and heat transfer in the downcomer during flow stagnation conditions are more accurately described as buoyancy opposed mixed convection. In this situation, heat transfer is from the hot walls to subcooled fluid flowing downward under low flow conditions. Under these conditions, heat transfer may be enhanced compared to free convection as modeled in RELAP5, which would promote more rapid cooling of the vessel walls.

Sensitivity studies utilizing the Petukhov correlation for parallel plates (known as the ORNL ANS Interphase Model in

RELAP5/MOD3.2.2Gamma) in lieu of the Dittus-Boelter correlation were performed. Additionally, RELAP5/MOD3.2.2Gamma was modified to apply a multiplier to compensate for buoyancy effects in forced turbulent convection published by Swanson and Catton [Swanson 87]. This model was later refined to utilize the Petukhov-Gnielinski heat transfer correlation along with the multiplier proposed by Swanson and Catton.

Other studies were performed where the heat transfer coefficient calculated by RELAP5 was varied by ±30%. The results of these RELAP5 calculations were analyzed using FAVOR to determine the direct impact of heat transfer uncertainty on vessel failure probability. The results of the heat transfer coefficient sensitivity studies are discussed in Chapter 9.

In-vessel circulation flows that deliver water from the upper plenum region to the upper downcomer can occur during a transient (particularly a LOCA). Such flows would tend to warm the water in the upper downcomer and the cold legs. Experiments and CFD studies have shown that there can be significant counter-flow of warm water from the upper downcomer, and energy exchange in the cold leg between the warm stream and the cold ECC injection. These in-vessel flows tend to increase the downcomer temperature.

The B&W vent valve design allows for significant in-vessel circulation once the reactor coolant pumps are tripped. While the pumps are on, the vent valves are held shut by differential pressure. After the pumps are tripped, flow stagnation conditions can occur, and the resulting pressure difference between the upper plenum and the downcomer will cause the vent valves to open, resulting in significant flow of warm water from the upper plenum to the downcomer. The impact of vent valve function on the downcomer fluid temperature is transient-dependent, but can be on the order of 50 K (90°F) based on a 2.83-in. (7.18-cm) surge line break, as seen in the next section.

While Westinghouse and CE plants do not have vent valves, they do have a bypass flow path between the upper downcomer and the upper plenum. The area of this path is generally not precisely characterized in power plants, but amounts to approximately 3% of the total core flow during normal plant operation. Assuming typical values of entrance and exit loss coefficients, the approximate flow area becomes 0.580-ft^2 (0.054-m^2) (10-in. [25.4-cm] diameter equivalent). This value is about 7% of the flow area of the Oconee vent valves, which is 8.45-ft^2 (0.785-m^2). The RELAP5 results were reviewed to evaluate bypass flows, for a large number of Palisades and Beaver Valley transients. The calculations indicate that the flow through the bypass region is small compared to the B&W vent valve flow, implying that the effect of bypass flow on downcomer temperature is small for Westinghouse and CE plants.

6.8.2 Treatment of Uncertainties

6.8.2.1 Overview

The approach used to address uncertainty in the thermal-hydraulic analysis principally utilized sensitivity studies to quantify the effect of phenomenological and boundary condition uncertainties/variations on the severity of a TH sequence. The results of these studies were used in either of the following two ways:

(1) They were combined with probability estimates on the sensitivity parameters being evaluated to adjust the bin probabilities from the PRA analysis.

(2) They were used to justify further subdivision of the PRA bins.

In this way, the TH uncertainty analysis accounted for certain parameters that can affect the thermal-hydraulic response of the plant that were not explicitly considered in the PRA analysis (e.g., season of the year). Because the uncertainty analysis also produced insights regarding the effects of various system parameters and TH models on event severity, it also helped to identify the transient used to represent each PRA bin to the PFM analysis.

Table 6.2 Summary of PTS Sensitivity Studies

Parameter	Significance	Sensitivity Evaluation	Results
Break flow (or valve capacity)	Most important factor in determining the RCS cooldown and depressurization rate. Directly impacts ECCS injection flow.	Break spectrum analysis performed for the three plants analyzed. Range of break diameters considered is 1-in. (2.54-cm) to 22-in. (56-cm), sequentially increasing the flow area by a factor of 2. Analyses where the flow area was varied by ±30% were also performed.	Significant effect on downcomer conditions. Can be significant contributor to vessel failure risk. Uncertainty in break flow for a given break area is small, given the range of break areas evaluated.
Break location	Downcomer temperature generally warmer for cold leg breaks vs. hot leg breaks. Hot leg breaks generally result in lower downcomer temperatures because the break flow enthalpy is higher for a hot leg break than for the same size cold leg break. In addition, for cold leg breaks, the ECC flow into the broken cold leg tends to flow out the break. Therefore, less cold ECC water is delivered to the downcomer.	Effect of break location evaluated by analyzing both cold leg and hot leg breaks.	Significant effect on downcomer conditions. Either hot leg or cold leg breaks can be significant contributors to vessel failure risk.
HPI Flow (BC)	ECCS flow rates are specified from pump flow curves which are pressure dependent.	HPI flow rate varied by ±10%. Evaluations also done considering HPI pump failure.	Effect of flow rate sensitivity found to have an insignificant impact on downcomer conditions and is not a significant contributor to vessel failure risk. Transients involving pump failure resulted in warmer downcomer temperatures, but are generally small contributors to vessel failure risk.

Parameter	Significance	Sensitivity Evaluation	Results
Accumulator Injection Temperature	Injection of large volume of cold water as the system pressure reaches the injection pressure of the accumulators. Injection temperature is dependent upon the season (winter or summer) assumed.	Temperature varied from 294 K (70°F) to 314 K (105°F) depending on the plant analyzed and season assumed.	Significant effect on downcomer conditions, principally temperature in conjunction with HPI and LPI injection temperature sensitivity evaluation. Can be significant contributor to vessel failure risk.
Accumulator Injection Rate	Injection of large volume of cold water as the system pressure reaches the injection pressure of the accumulators.	The effect of pressure on flow was examined by varying the initial pressure from 3.8 MPa [550 psi], 4.1 MPa [600 psi] (nominal) and 4.5 MPa [650 psi].	Insignificant effect on downcomer conditions.
HPI and LPI Injection Temperature	Seasonal effect on the injection water temperature, which affects the downcomer water temperature. Done in conjunction with the accumulator injection temperature sensitivity.	Oconee – Temperature range considered is 278 K (40°F) to 303 K (85°F). Palisades – Temperature range considered is 278 K (40°F) to 311 K (90°F). Beaver Valley – summer temperature of 286 K (55°F) considered. Note that Beaver Valley maintains ECC water temperature at a constant 300 K (50°F) in accordance with Technical Specifications.	Significant effect on downcomer conditions. Affected transients can be significant contributors to vessel failure risk.
Decay Heat Load	Decay heat load directly affects downcomer conditions.	Hot full power conditions and hot zero power conditions considered. Hot zero power defined as 0.2% of full core power (~5.2 MWth).	Uncertainties in decay heat load small compared to the range of conditions considered.
HPI Flow Control	Direct impact of HPI flow rate on downcomer conditions. HPI throttling generally reduces downcomer temperature and system pressure.	For transients involving either closure of a stuck-open pressurizer SRV or main steam line break, the RCS may reach conditions for which operating procedures require HPI throttling or termination. For these transients, the scenarios analyzed varied the timing and conditions under which the operator controlled HPI flow.	Significant effect on downcomer conditions, principally temperature. Affected transients can be significant contributors to vessel failure risk.

Parameter	Significance	Sensitivity Evaluation	Results
Feedwater Control	Direct impact on downcomer conditions particularly if the steam generator is overfilled.	Various feedwater control scenarios ranging from normal control of steam generator level to failure of level control or operator error, resulting in filling of the steam generators until water entered the steam lines.	Range of sequences analyzed covers uncertainty in feedwater control. Generally, effects are insignificant unless combined with a valve failure or MSLB.
Secondary Pressure Control	Direct impact on downcomer conditions for MSLB or stuck-open secondary relief valve sequences.	A spectrum of PRA sequences were analyzed for failures of secondary side valves, including steam dump, steam generator safety/relief, and atmospheric release valves. The failures were combined in some instances with failure of feedwater control such that the faulted steam generator continued to be fed with auxiliary feedwater.	Significant effect on downcomer conditions. Affected transients can be significant contributors to vessel failure risk.

This method of accounting for TH uncertainty does not quantify the uncertainties associated with each TH sequence; rather, it characterizes the uncertainties associated with each PRA bin. This is appropriate because, as illustrated in Figure 3.3, each TH sequence that is passed on to the PFM analysis represents a much larger number of TH sequences that, together, constitute a PRA "bin." Provided the combined effects of the TH parameter and modeling uncertainties on the severity of this one representative sequence is small relative to both

- the uncertainty in the frequency of occurrence of all of the sequences in the bin, and
- the variability in severity between the different sequences in the bin, then

the uncertainty associated with TH parameter and modeling uncertainties of the representative sequence can be considered negligible. The appropriateness of not accounting for these uncertainties because they are negligibly small is ensured by the iterative process used to define the PRA bins. PRA bins that contribute significantly to the estimated TWCF were continually partitioned (including appropriate partitioning of their frequencies and selection of new TH sequences to represent each partitioned bin) until the total estimated TWCF for the plant did not change significantly with continued partitioning. Thus, any errors caused by not explicitly accounting for the TH parameter and modeling uncertainties associated with the TH sequence used to represent each PRA bin are not expected to influence the outcome of the analysis (i.e., the estimated values of TWCF).

The following section summarizes the TH uncertainty analysis. Full details can be found in a companion report [***Chang***].

6.8.2.2 Approach

The TH uncertainty characterization begins with identification of the event categories (e.g., LOCAs) that are expected to significantly challenge vessel integrity. If necessary, each of these event categories was then subdivided. For example, the LOCA event category called was subdivided as follows:

- Small LOCA: between 1.5-in. (3.8-cm) and approximately 4-in. (10-cm)
- Medium LOCA: approximately 4-in. (10-cm) and approximately 8-in. (20-cm)
- Large LOCA: greater than approximately 8-in. (20-cm)
- Stuck-open pressurizer safety relief valves
  - Without subsequent reclosure
  - With subsequent reclosure, resulting in system repressurization

The aim of event category subdivision was to better bound the uncertainty by not having one category attempt to represent too broad a range of thermal-hydraulic conditions. However, even within these subdivided event categories the response of the plant can vary due to sequence to sequence differences within each subdivision. To quantify this, the following uncertainties were identified:

- Aleatory Uncertainties
  (1) Break diameter (1- to 22-in. (2.5- to 56-cm)): variation of ±30% considered.
  (2) Break location (surge line or hot leg, cold leg)
  (3) Decay heat level (full power, low (hot zero) power)
  (4) Reactor coolant pump status (tripped vs. operating)
  (5) Heat structure sensible heat (variation of ±30% considered)
  (6) HPI state (normal operation, failed)
  (7) HPI flow rate (±10%)
  (8) Accumulator pressure ± 345 kPa (±50 psi), accumulator temperature: 21°C, 43°C (70°F, 110°F)
  (9) Effect of seasonal variation on downcomer temperature (summer, winter)
- Epistemic Uncertainties
  (1) In-vessel circulation attributable to vent valve function in Oconee (cases where valves failed were considered)
  (2) Vessel wall-to-downcomer fluid heat transfer
  (3) Flow resistance (loop flow)
  (4) Break flow

6.8.2.2.1 Break Diameter and Location (Aleatory 1 and 2)

Downcomer conditions are strongly influenced by the break diameter (break flow) and break location. Various diameters (1.5-in. (3.8-cm) to 22-in. (56-cm)) and break locations (surge line, hot leg, and cold leg) are considered.

The thermal-hydraulic response of the reactor system is considerably different as the break diameter increases from 2-in. (5.08-cm) to 16-in. (40.64-cm). For the larger break cases of 8-in. (20.32-cm) or more, maximum ECCS delivery will occur (the HPI and LPI systems will be operating at pump runout conditions), resulting in the maximum rate of reactor coolant system (downcomer) cooldown and depressurization.

For smaller breaks in the range of 5.6-in (14.37-cm) or less, ECCS delivery flow will be limited by the break flow so that the rate at which reactor coolant system cooldown and depressurization will occur is more strongly tied to break diameter and location. In this range, the rate of reactor system cooldown and depressurization decreases with break diameter. Transients involving stuck-open primary side safety valves fall into this category.

ECCS performance is also affected by the break location. For hot leg or surge line breaks, the ECCS will flow from the cold legs through the downcomer to the break. For cold leg breaks, some of the ECCS flow will be discharged through the break.

Inherently, the rate of reactor system cooldown and depressurization is more uncertain in this range relative to break diameters greater than 8-in. (20.32-cm). Hence, the uncertainty analysis focused on break diameters less than 5.6-in (14.37-cm). A ±30% variation on break area to account for break flow uncertainty was considered for LOCA and stuck-open primary safety valve transients.

6.8.2.2.2 Heat Sources (Aleatory 3, 4, and 5)

Heat sources affecting downcomer conditions include the decay heat load, reactor coolant pump status, and the sensible heat in the reactor plant heat structures.

In the case of decay heat load, three sets of decay heat data corresponding to full-power operation, 0.7% of full-power operation, and 0.2% of full-power operation were analyzed. Later in the analysis, the low-power operations were combined into the hot zero power initiating state. Probabilities assigned to these states are 0.98 for hot full-power conditions and 0.02 for hot zero power conditions. Uncertainties in heat load due to RCP operation were considered by evaluating transients where the pumps are tripped vs. when they remain operating.

The principal effect of sensible heat in the heat structures is the rate at which heat is transferred from the system structure to the system fluid. A range of ±30% is considered in the uncertainty analysis.

6.8.2.2.3 High-Pressure Injection (Aleatory 6 through 9)

ECCS performance considered four factors, including (1) failure on demand, (2) injection flow rate, (3) injection temperature, and (4) injection timing. System failures include a partial or full system failure, where the injection flow at the required rate is not delivered. Failures of this type result in warmer downcomer temperatures. Transients involving HPI failure have been considered in the uncertainty analysis. Flow rate uncertainty was assessed using a ±10% variation in HPI flow. Flow rate uncertainties in the LPI or accumulators (or core flood tank) were also considered.

Uncertainty in injection temperature considers the effect of seasonal variations on the injection water source, which is the refueling water storage tank located outdoors. Table 6.2 lists the values used. Probabilities assigned to the

seasonal variation are 0.25 for summer and winter and 0.50 for fall/spring. Uncertainty in injection timing of the accumulators was considered by varying the injection pressure over a range of ±50 psi. The pressures at which high- and low-pressure injection is initiated are judged to have a small uncertainty. Uncertainty in the RCS coolant loop total flow resistance focuses on the loop flow resistance. A 100% increase in flow resistance was considered.

6.8.2.2.4 Vent Valves (Epistemic 1)

Uncertainty in the in-vessel circulation, which affects the energy distribution in the reactor coolant system, focuses principally on Oconee because of the presence of the vent valves. For the uncertainty evaluation, failure of the valves to open was considered.

6.8.2.3 Definition of Sensitivity Indicator

Sensitivity analyses were performed with RELAP5 for each of the parameters discussed in Section 6.8.2.2. Downcomer temperature is the most important of the three thermal-hydraulic boundary conditions in the fracture analysis and therefore is the focus of the sensitivity analysis. The sensitivity indicator is the effect on the average downcomer temperature due to the change in a single sensitivity parameter over the transient time of interest, which is 10,000 seconds for this analysis. Each sensitivity indicator has an associated probability of occurrence determined from the parameter being varied. The following equation is used to compute the sensitivity indicator:

$$\Delta T = \overline{T}_{sen} - \overline{T}_{nom}$$

where $\overline{T}_{sen}$ is the sensitivity case downcomer temperature averaged over the 10,000 seconds interval and $\overline{T}_{nom}$ is the base case downcomer temperature averaged over the 10,000 second interval. To compute the sensitivity indicator, each sensitivity parameter is varied (one at a time) to an upper and lower bound and the average temperature difference is determined. This approach is called the nominal range sensitivity analysis and is described in more detail in [***Chang***].

The impact on the sensitivity indicator of a given sensitivity parameter depends strongly on the transient and therefore a large number of transients that include the types of transients considered in the PTS analysis (LOCAs, stuck-open primary safety valves, MSLBs, etc.) need to be considered.

6.8.2.4 Example of Results for a Surge Line Break

The case of a 2.83-in. (7.18-cm) surge line break LOCA for Oconee is used to illustrate the development of the sensitivity indicator. Figure 6.28 presents the sensitivity parameter ranking for the 2.83-in. (7.18-cm) surge line break LOCA for Oconee. For this case, the sensitivity indicator ranges from an increase of 100K (180°F) when HPI is assumed to fail to a decrease of 35 K (63°F) for hot zero power initialization. The sensitivity indicator depends on the transient being considered and sensitivity indicators were developed for the range of transients considered in the PTS analysis.

The uncertainty evaluation requires consideration of the effect of multiple parameters on the downcomer conditions. As an example, a transient may be initiated from hot zero power during the summertime. The sensitivity studies only evaluated the effect of increasing or decreasing a single parameter. To combine the effect of multiple parameters on the downcomer fluid temperature, the sensitivity indicators are added together. This approach is based on the assumption that the effect of any sensitivity parameter is independent of the effect of any other parameter so that the sensitivity indicators become linearly additive. Application of the linearly additive assumption avoids performing RELAP5 sensitivity studies on the large number of sensitivity parameter combinations. The linear additive assumption was applied to the various types of transients considered in the uncertainty analysis.

Validation of the linear additive assumption (LAA) was done by varying multiple sensitivity parameters in a single RELAP5 run based on a 2.83-in. (7.18-cm) surge line break LOCA model for Oconee. Five different combinations of sensitivity parameters were selected to cover a downcomer temperature range of 111 K (200°F).

Table 6.3 lists the five combinations of sensitivity parameters considered and the results of T_{sens} computed applying the linear additive assumption compared to direct computation using RELAP5. A plot of the results is shown in Figure 6.29. The 45-degree line in Figure 6.29 represents the perfect scenarios in which the expected values are same as the RELAP5 calculated values. The solid dots represent the realities. The difference between the solid dots and the squares on the 45-degree line is the deviation of the LAA from the RELAP5 results. Figure 6.29 shows that downcomer temperature computed using the linear additive assumption is in good agreement with the RELAP5 calculated results.

Given the important sensitivity indicators and associated probabilities, a statistical analysis is carried out to finalize selection of representative transients for each bin and to refine the frequencies for the bins defined during the front-end risk modeling. This statistical analysis is performed in two parts. First, the downcomer temperature is determined by adjusting the nominal downcomer temperature for each subcategory identified in Step 5 by the sensitivity indicator (downcomer temperature adjustment) for all combinations of sensitivity parameters being considered for that subcategory using the linear additive approach. Then, the probability of occurrence for each combination of sensitivity parameters is determined. Note that thousands of temperature points are generated for all of the combinations of sensitivity parameters considered.

Table 6.3 List of Combined Sensitivity Indicators Varied for LAA Verification

No.	Sensitivity Parameters Varied	T_{sens} using LAA	T_{sens} (°K) using RELAP5	$T_{sens,RELAP5} - T_{sens,LAA}$ (°K)
1	Winter conditions; p(CFT) +50 psi; 70% A_{brk}; RVVVs Close; 70% HTC	331.7	345.3	13.6
2	Summer; vent valves failed closed; 200% loop flow resistance	360.0	362.3	2.7
3	p(CFT) +50 psi; 110% nominal HPI mass flow; 70% nominal break area; 130% nominal heat transfer coefficient	387.6	391.4	3.8
4	Summer conditions; p(CFT) +50 psi ; 90% nominal HPI mass flow; 130% nominal break area; normal vent valve function; 200% loop flow resistance	415.5	406.9	-8.6
5	Summer conditions; 90% nominal HPI mass flow; 70% nominal break area; normal vent valve function; 130% nominal heat transfer coefficient.	438.2	448.8	10.7

Given the downcomer temperature and corresponding probability, a probability density function is constructed. The development of this function is illustrated in Figure 6.30 for Oconee for LOCAs between 1.5-in. (3.81-cm) and 4-in. (10.16-cm) in diameter. This figure shows the resulting cumulative distribution function found from integrating the probability density function that is used to obtain the probabilities used to adjust the bin frequencies.

The representative scenarios are determined from the probability density function by subdividing the probability into five bands between the 0.05 and 0.95 probability levels and determining the temperature at the median point in each band. The probabilities in the two regions near the tails are increased by 0.05. This adjustment is made because of potentially large errors in the sensitivity indicator in the tails of the probability density function (below 0.05 and above 0.95 probability level). In Figure 6.30, there are five bands shown on the cumulative density function plots along with the median values identified and the downcomer temperature corresponding to each median.

Selection of the representative scenario corresponding to the median temperature in each probability band in the cumulative density distribution plot is done by picking the sensitivity indicator result that corresponds to the median temperature and using the corresponding set of RELAP5 results for probabilistic fracture mechanics analysis. An example of the selection of representative scenarios along with the corresponding probabilities is presented in Table 6.4.

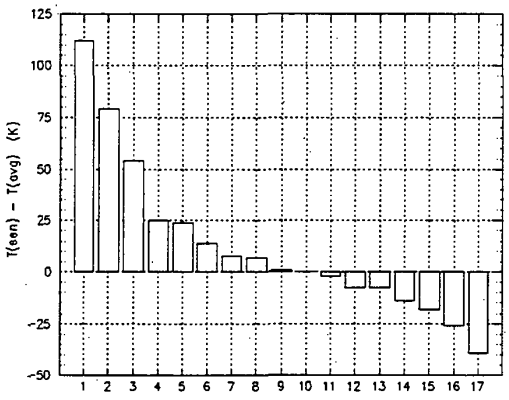

The uncertainty analysis was performed for the transients considered for the Oconee, Beaver Valley, and Palisades plants. There were some variations in the thermal-hydraulic categories considered, the sensitivity indicators evaluated and in the set of representative transients selected. These variations are attributable to differences principally in plant design and plant operating conditions. Otherwise, the approach used is the same for the three plants. Adjustments were made to the bin probabilities and representative sequences were selected based on the uncertainty analysis conducted for the three plants. Details can be found in [***Chang***].

1	100% HPI fail
2	50% HPI fail
2	50% HPI fail
3	25% HPI fail
4	RVVVs Open
5	CL LOCA
6	90% m(HPI)
7	130% CHTC
8	Summer
9	P(CFT) -= 50 psi
10	Nominal
11	P(CFT) += 50 psi
12	110% m(HPI)
13	70% CHTC
14	Winter
15	High CL rev. K
16	RVVV Close
17	HZP

Figure 6.28. Sensitivity parameter ranking of a 2.8-in. (7.18-cm) surge line break LOCA

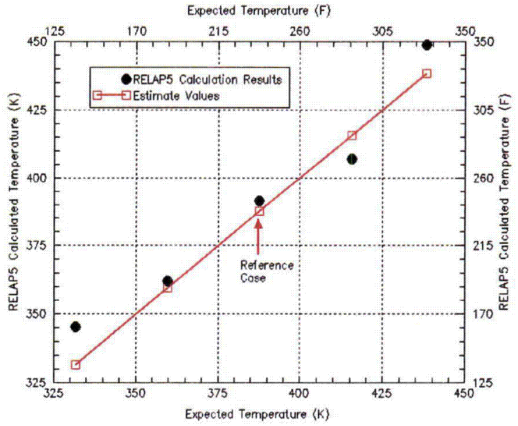

Figure 6.29. Confirmation of the Linearly Additive Assumption for a 2.8-in. (7.18-cm) surge line break LOCA

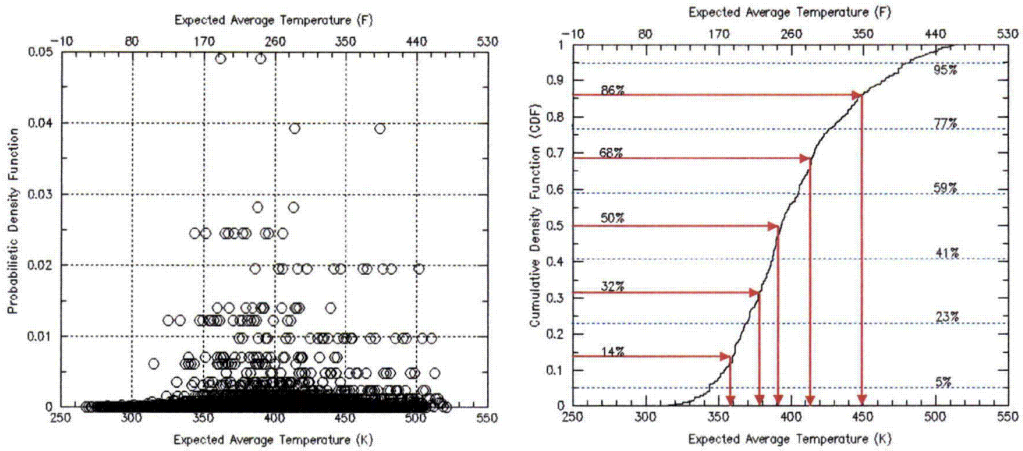

Figure 6.30. Illustration of the Statistical Results for Downcomer Temperature Distribution

Table 6.4 Example of Representative Scenario Selection

#	TH Bin #	Probability	Scenario Specification Descriptions
1	145	0.23	1E-3 m^2 cold leg LOCA with increased 30% break area (Winter)*
2	142	0.18	4E-3m^2 surge line with 30% reduced break area
3	141	0.18	4E-3m^2 surge line with 30% increased break area
4	172	0.18	8E-3m^2 cold leg LOCA
5	154	0.23	8E-3m^2 surge line LOCA with 30% reduced break area RPV vent valves closed

7 Probabilistic Fracture Mechanics Analysis

7.1 Interaction of PFM Model with PRA and TH models

Figure 7.1 illustrates how the PFM model connects to both the PRA and TH models discussed in Chapters 5 and 6, respectively. Specifically, the PFM model takes as input from TH the pressure, temperature, and heat transfer coefficient time histories that have been defined by TH for the sequences defined by PRA. The PFM model uses this TH information along with other information concerning plant design and materials of construction to estimate the time-dependent driving force to fracture produced by a particular event sequence. The PFM model compares this estimate of fracture driving force to the fracture toughness, or fracture resistance, of the RPV steel. This comparison allows us to estimate the probability that a particular sequence of events will produce a crack all the way through the RPV wall were that sequence of events actually to occur. The final step in the analysis involves a matrix multiplication of these through-wall cracking frequency estimates with the frequency at which a particular event sequence is expected to occur (as defined by PRA). This product establishes an estimate of the annual frequency of through-wall cracking that can be expected for a particular plant after a particular period of operation when subjected to a particular sequence of events. The annual frequency of through-wall cracking is then summed for all event sequences specified by PRA to estimate the total annual frequency of through-wall cracking for the vessel. Performance of such analyses for various operating lifetimes provides an estimate of how the annual through-wall cracking frequency can be expected to vary over the lifetime of the plant.

7.2 Components of the PFM Model

Figure 7.1 also shows that the PFM model is itself composed of four major sub-models (which themselves are composed of yet more sub-models and parameter inputs). The four major sub-models that make up the PFM model are as follows:

- A flaw distribution model: see Section 7.5 for an overview and [***Simonen***] for details.
- A neutronics model: see Section 7.6 for an overview and [***EricksonKirk-PFM***] for details.
- A crack initiation model: see Section 7.7 for an overview and [***EricksonKirk-PFM***] for details.
- A through-wall cracking model: see Section 7.8 for an overview and [***EricksonKirk-PFM***] for details.

Together, these four sub-models provide the information necessary to estimate both the fracture driving force ($K_{applied}$) generated by the PTS loading and the resistance of the material to fracture ($K_{Resistance}$). $K_{applied}$ depends upon the thermal-hydraulic inputs of pressure, temperature, and heat transfer coefficient (all *vs.* time), on the vessel dimensions, and on the location and size of the flaws that are quantified by the flaw distribution model. $K_{Resistance}$, more commonly called "fracture toughness," depends upon the chemical composition of the steel, the downcomer temperature from the thermal-hydraulics calculations combined with the heat conduction properties of the steel, and on the degree of neutron irradiation exposure experienced by the steel. Our calculations consider the potential for cracks to initiate in either a brittle manner by cleavage or in a ductile manner by microvoid initiation and coalescence. (The type of crack initiation that occurs depends upon the temperature.) We also consider the

potential for cleavage cracks to stop, which is a phenomenon referred to as "crack arrest." These different failure modes all have different characteristics fracture toughness ($R_{esistance}$) values, as follows:

- K_{Ic} quantifies the resistance of the material to crack initiation in cleavage.
- J_{Ic} and J-R quantifies the resistance of the material to crack initiation by micro-void coalescence. Furthermore, the J-R curve describes the resistance of the material to further ductile crack growth.
- K_{Ia} quantifies the ability of the material to stop (arrest) a running cleavage crack.

These various values of $K_{Resistance}$ (K_{Ic}, J_{Ic}, J-R, and K_{Ia}) and their dependencies on chemical composition, temperature, and neutron irradiation exposure are estimated by a combination of the neutronics model, the crack initiation model, and the through-wall cracking model. Also, the crack initiation model and the through-wall cracking models estimate, respectively, the probability of crack initiation and the probability of through-wall cracking by comparing the value of $K_{applied}$ to the appropriate value of $K_{Resistance}$.

7.3 Objectives of this Chapter

The objectives of this chapter are as follows:

(1) Section 7.4: Describes our approach to model development and uncertainty characterization.

(2) Sections 7.5 through 7.8: Provide a summary discussion of the four major sub-models that make up the PFM model.

(3) Section 7.9: Provides a summary discussion of how all of these sub-models are implemented in the FAVOR probabilistic fracture mechanics code. (See [***Dickson-UG***] and [***Williams***] for details.)

(4) Section 7.10: Provides a summary discussion of an experimental validation of the linear elastic fracture mechanics (LEFM) techniques that underlie our approach. (See Appendix A of [***EricksonKirk-PFM***] for details.)

7.4 Approach to Model Development and Uncertainty Characterization

As discussed in Section 3.2, our approach to developing a risk-informed revision of 10 CFR 50.61 requires explicit identification of the type of uncertainty (aleatory or epistemic) to enable the development of an appropriate mathematical model. To do so, it is first necessary to establish independent, physically motivated, models that account for the effects of irradiation damage and temperature. We achieved this goal by the following three-step process:

(1) Uncertainty Identification: We began by constructing a graphical description of the current toughness model. This description, called a "root cause diagram," is illustrated schematically in Figure 7.2. Diagrams of this type show *all* of the parameters (shaded boxes) and *all* of the relationships (nodes) used to estimate the fracture toughness for a particular set of conditions. Decomposing the toughness / embrittlement model in this way permitted identification of individual sources of uncertainty, both in the parameters and in the relationships assumed between the parameters.

(2) Uncertainty Classification: Uncertainties were classified through an understanding of the basic physical mechanisms responsible for crack initiation, for crack arrest, and for irradiation damage. Without this physical understanding, it was impossible to distinguish the irreducible (i.e., aleatory) uncertainties associated with variability of the material from reducible (i.e., epistemic) uncertainties caused by limited data, imperfect models, and so on.

(3) Uncertainty Quantification: The physical understanding developed to classify uncertainty types also played a pivotal role in uncertainty quantification because a model of fracture toughness that can be regarded as representing the true behavior

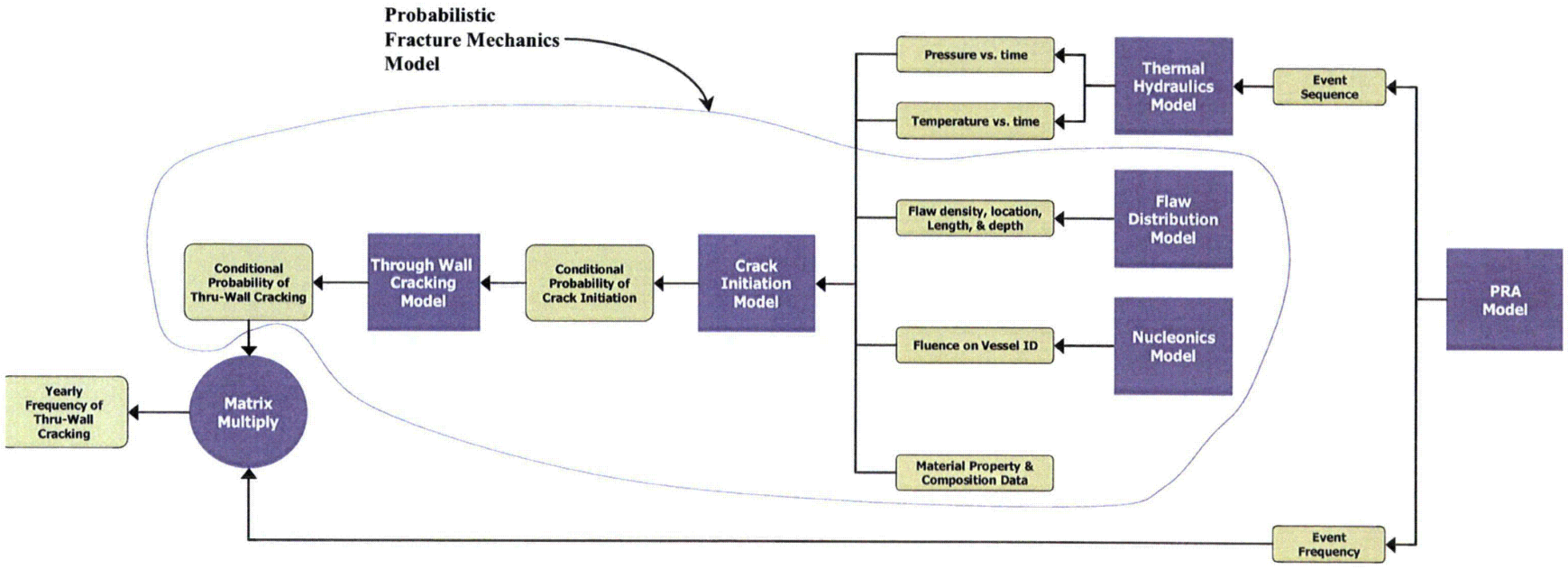

Figure 7.1. Illustration of the interrelationships between PFM model and the TH and PRA models, and the four principal sub-models that comprise the PFM model

of the material is needed to quantify the uncertainties present in any other model. Therefore, uncertainty quantification was achieved by comparing the RT_{NDT}-based toughness model developed for use in the PTS reevaluation project to this best-estimate model.

To be consistent with LEFM principles, LEFM-valid K_{Ic} and K_{Ia} values were used to calibrate the parameters of this best estimate model. However, the best-estimate model cannot be constructed as a purely empirical fit to these K_{Ic} and K_{Ia} values. Without the insights available from a physically based understanding it was impossible to discern if the trends demonstrated by the laboratory data can be expected to apply to the material and loading conditions of interest in commercial PWRs. Consequently, the "best estimate models" each had a form motivated by the physical processes responsible for the underlying phenomena.

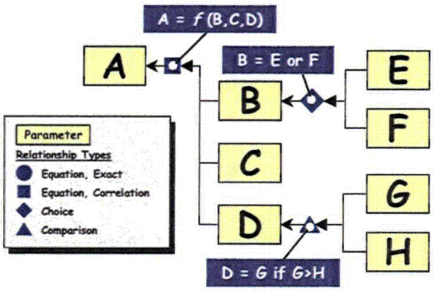

Figure 7.2. Illustration of a root cause diagram showing how uncertainties in input variables (E, F, G, and H) propagate through models (nodes), themselves potentially having uncertainty, to produce uncertainty in a resultant value (A)

7.5 Flaw Model

The flaw model provides estimates of the density (flaws per unit area or volume), size, and location in the vessel wall of initial fabrication defects[‡‡]. This flaw distribution, reported in detail by [***Simonen***], represents a major improvement in realism relative to that adopted in previous studies of PTS risk. Indeed, one of the major unknowns/uncertainties identified in the last comprehensive evaluation of PTS [SECY-82-465] was the distribution of flaws assumed to exist in the RPV wall. SECY-82-465 used flaw models based on the Marshall study, which included data from a limited population of nuclear vessels and from many non-nuclear vessels [Marshall 82]. These flaw measurements were part of routine pre-service NDE examinations performed 25 or more years ago at vessel fabrication shops. Given the limitations of the NDE technology available at the time, the Marshall flaw distribution provides a reasonable representation only for flaws having depth dimensions larger than ≈1-in. (2.54-cm). The Marshall distribution was nonetheless applied in SECY-82-465 and in the IPTS studies [ORNL 85a, 85b, 86] by extrapolating fits to the data to the much smaller flaws of concern in PTS calculations (less than ≈0.25-in. (0.64-cm)). Additionally, all flaws in the Marshall distribution were assumed to break the inner-diameter surface of the RPV despite the fact that the observations rarely, if ever, revealed surface breaking flaws in nuclear grade construction.

Table 7.1 summarizes the various sources of experimental data used by Simonen et al. to develop the flaw distributions used in FAVOR. While the volume of material represented in Table 7.1 improve greatly on the Marshall flaw distributions [Marshall 82], an inescapable conclusion is also that the quantity of available data is also quite small compared with the volume of RPV material in service. Consequently, it is not possible to ensure on an empirical basis alone that the flaw distributions developed based on these data apply to all PWRs in general. However, the flaw distributions proposed in [***Simonen***] rely on the experimental evidence gained from inspections of the materials summarized in Table 7.1 do not rest solely on this empirical evidence. Along with these data Simonen et al. used both physical models and expert opinions when developing their recommended flaw distributions. Additionally, where detailed

‡‡ Growth of initial fabrication defects attributable to sub-critical cracking mechanisms does not need to be considered; see Section 3.3.3.2.

information was lacking Simonen et al. made conservative judgments (for example, all NDE indications were modeled as cracks and, therefore, potentially deleterious to RPV integrity). This combined use of empirical evidence, physical models, expert opinions, and conservative judgments allowed Simonen et al. to propose flaw distributions for use in FAVOR that are believed to be appropriate/conservative representations of the flaw population existing in PWRs in general. (See Appendix C and [***Simonen***] for details.)

Table 7.1. Summary of sources of experimental data sources for the flaw distribution

Vessel	Weld	Plate	Clad
PVRUF	9150	855	1650
Shoreham	10375	975	--
Hope Creek	245	550	--
River Bend	2440	1465	--

Table entries represent volume of material examined in in^3.

In the following sections, we summarize the findings of this study for buried flaws in welds (Section 7.5.1), buried flaws in plates (Section 7.5.2), and surface flaws in both plates and welds (Section 7.5.3). Section 7.5.4 contrasts our flaw distribution the results with the Marshall distribution used in SECY-82-465.

7.5.1 Buried Flaws in Welds

The Simonen study made the following observations regarding flaws that form as part of the axial or circumferential weld fabrication process:

(1) Flaws in welds are distributed uniformly through the thickness of the RPV weld. There is no tendency for a greater density of flaws to occur either near the root or cap passes.

(2) No surface breaking flaws were identified in all of the weld material examined, nor was a credible physical mechanism for surface flaw generation identified. Consequently, the flaw distributions used herein contain *only* buried flaws. This is a significant change from the Marshall flaw distribution, which contained *only* surface breaking flaws.

(3) Virtually all non-volumetric flaws found in welds were lack of side-wall fusion defects that exist on the fusion line between the deposited weld metal and the plate or forging being joined. Consequently, the number of flaws in a particular weld scales in proportion to the fusion line area. Additionally, this observation implies that axial welds contain *only* axially oriented flaws whereas circumferential welds contain *only* circumferentially oriented flaws.

(4) Data on flaw density exhibited statistically significant differences depending upon the welding process used (SAW, SMAW, GMAW, or repair weld). However, it is difficult in practice to ascertain from records precisely where different weld processes were used, or where repair welds were made. For this reason, we decided that the flaw distributions used in this study would represent blended combinations of the SAW, SMAW, and REPAIR flaw distributions. Percentages of SAW and SMAW were established on a vessel specific basis. The percentage of repair weld was assumed to be 2% for all vessels analyzed. A repair weld volume of 2% exceeds slightly the repair percentage of 1.5% that was observed by PNNL for both the Shoreham and PVRUF vessels.

(5) Flaw densities exhibited statistically significant differences depending upon the vessel examined (PVRUF or Shoreham). Since Simonen did not establish a model capable of explaining why the density and size of flaws can be expected to vary from vessel to vessel, it was decided to adopt for FAVOR calculations flaw densities based only on observations of the Shoreham vessel because the Shoreham welds had a higher flaw density than the PVRUF welds.

(6) Flaw depth dimensions did not exhibit statistically significant differences for the different welding process and vessels examined, so in this case the data from the different processes and vessels were pooled.

There was, however, clear differences in the distributions of flaws length depending on the welding processes and vessels examined, so the flaw length distributions were established on a case-by-case basis.

It should also be noted that the empirical data used as the primary evidence to establish the distribution of embedded weld flaws do not, and cannot, provide any information about the maximum size a flaw can be. For this reason, it was decided to truncate the non-repair flaw distribution at 1-in. (2.54-cm) and the repair flaw distribution at 2-in. (5.08-cm). In both cases, the selected truncation limit exceeds the maximum observed flaw size by a factor of 2. We performed a sensitivity study with FAVOR and ascertained that, within reasonable bounds on truncation limit dimension, the estimated through-wall cracking frequency is not influenced in any significant way by the truncation limit [Dickson 03].

7.5.2 Buried Flaws in Plates

As reflected by the information in Table 7.1, the empirical evidence available to support a plate flaw distribution is much more limited than the available information for welds. Data on flaw rates and sizes from these sources agree well with two flaw distributions for plates derived by applying flaw density adjustment factors to weld flaw distributions. These adjustment factors, which were proposed by a group of experts [***Simonen***], are as follows:

- The density of plate flaws of depth less than 0.24-in. (6-mm) is 10% of that for weld flaws.
- The density of plate flaws of depth above 0.24-in. (6-mm) is 2.5% of that for weld flaws.

Since reasonable agreement exists between the limited experimental data on plate flaws and the adjusted weld distributions it was decided to use the adjusted weld distributions as input to FAVOR. A truncation limit of 0.43-in. (1.09-cm) was selected because it exceeds the largest observed plate flaw by a factor of 2. Again, a FAVOR sensitivity study demonstrates that this truncation limit does not influence significantly the estimated TWCF [Dickson 03].

Finally, the data reported by [***Simonen***] failed to reveal any preferred orientation for plate flaws. To model this finding in the most accurate way possible without performing mixed-mode fracture calculations, half of the simulated plate flaws are orientated axially, while the remaining half are oriented circumferentially in the vessel.

7.5.3 Surface Flaws in Welds and Plates

The entire inner-diameter of a nuclear RPV is clad with a thin layer of stainless steel to prevent corrosion of the underlying ferritic steel. Lack of inter-run fusion (LOF) can occur between adjacent weld beads, resulting in circumferentially oriented cracks. (All cladding in RPVs was deposited circumferentially.) While the data in [***Simonen***] shows a high probability (1 to 10 flaws per meter of deposited cladding weld bead) of obtaining very shallow LOF defects (1% of the clad layer thickness), only two deep LOF defects, having depths of ~50% and ~63% of the clad layer thickness, were found in all of the cladding inspected. Simonen found no evidence of LOF defects that completely compromised the clad layer.

The only flaws we expect to challenge the integrity of the RPV during PTS loading are those that completely penetrate the clad layer because it is only in this situation that the crack has its tip residing in the ferritic RPV steel, which is subject to neutron irradiation embrittlement. Despite the lack of empirical evidence for such deep flaws, it was not believed appropriate to completely exclude such flaws from the flaw model used in our PFM analysis owing to the limited amount of clad material examined. For this reason, we developed a distribution for small *buried* cladding flaws based on a combination of the data available, expert judgment, and the predictions of the PRODIGAL weld flaw simulation code [PRODIGAL]. This distribution was adjusted as follows to estimate the number of the clad flaws that fully penetrate the cladding thickness:

- We estimated that only $1/1000^{th}$ of the observed density of *buried* cladding flaws would fully penetrate the cladding thickness.

- We assumed that these surface breaking defects exist only in single layer cladding. Multi-layer cladding was assumed to have no surface breaking flaws because the likelihood of two LOF defects aligning in two different weld layers is quite remote.
- Based on the physical mechanism of their formation, all LOF defects are aligned with the clad welding direction (circumferential).

In FAVOR, these surface-breaking circumferential flaws in the cladding can be simulated to occur anywhere in the vessel (i.e., in any weld, plate, and forging).

7.5.4 Comparison of the Current Flaw Distribution with that Proposed by the Marshall Committee

Figure 7.3 compares of the Marshall flaw distribution with the three components of the flaw distribution developed by Simonen. The following observations can be made:

- In general, the individual contributions to the new flaw distribution contain more flaws than the Marshall distribution, but the flaws in the new distribution are considerably smaller.
- While all of the flaws in the Marshall distribution are surface-breaking, only flaws associated with the cladding are surface-breaking in our new distribution, and these comprise only a small percentage of the total. Also, these cladding flaws are all circumferentially oriented because they follow the direction of weld deposition.
- The Marshall distribution focused on flaws in welds and did not distinguish between flaws in different product forms. The new distribution does, and it demonstrates that flaws in base metal are considerably smaller and occur less frequently than flaws in welds.

As illustrated in Figure 7.4, Dickson and Simonen report that the estimated TWCF drops by a factor of between 20 and 70 when the new flaw distribution is adopted instead of the Marshall distribution [Dickson 03].

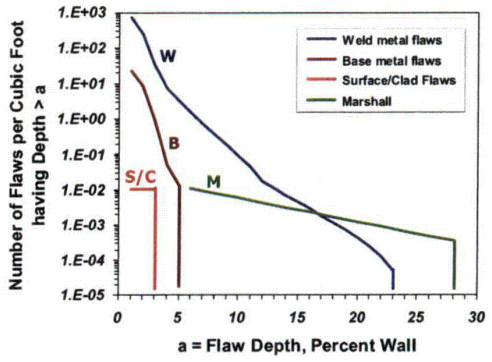

Figure 7.3. Comparison of the new flaw distribution to the Marshall flaw distribution

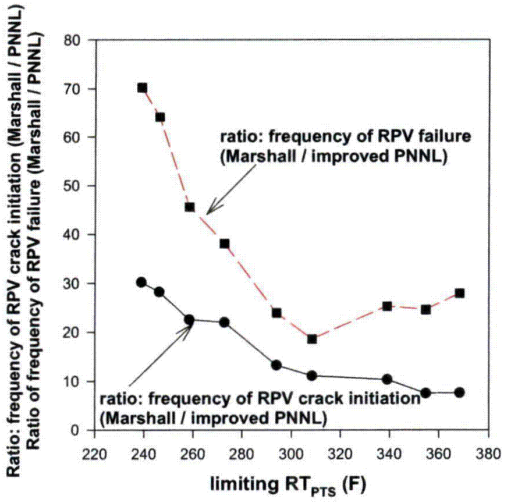

Figure 7.4. Illustration of the impact of the flaw distribution adopted in this study (improved PNNL) with that used in previous PTS calculations (Marshall flaw characterization) [Dickson 02] (analysis performed on Oconee at 60 EFPY)

7.6 Neutronics Model

The neutronics model is itself composed of two major components:

- a calculation of the fluence on the ID of the vessel performed according to NRC Regulatory Guide 1.190 [RG 1.190]
- attenuation of this fluence through the wall of the vessel to the location of the crack of

interest using the attenuation formula in Regulatory Guide 1.99 [RG 1.99].

7.6.1 ID Fluence

The variation of fluence over the inner diameter of the vessel is estimated using modeling procedures based on the guidance provided in the NRC Regulatory Guide 1.190 [RG 1.190], "Calculational and Dosimetry Methods for Determining Pressure Vessel Neutron Fluence." Fluences so calculated are considered best estimates because they are based on the most up-to-date calculational procedures.

While procedures used to calculate fluence have been updated from those that provided the basis of the current PTS Rule, the more significant change in our fluence treatment has been the refinement of our discretization of the circumferential and azimuthal variation of fluence. In previous studies, each major region in the beltline of the vessel (i.e., each weld, plate, or forging) was assigned a value of fluence equal to the peak value estimated to occur anywhere in the region. In contrast, our models capture the detailed azimuthal and axial variation of fluence, resulting in a much more realistic model of the fluence variation in the beltline region.

7.6.2 Through-Wall Fluence Attenuation

Similar to previous PTS calculations [SECY-82-465, ORNL 85a, ORNL 85b, ORNL 86] FAVOR adopts the Regulatory Guide 1.99, Revision 2, model of fluence attenuation through the thickness of the vessel [RG 1.99]. This model assumes that the fluence (and thus the damage caused by irradiation) drops exponentially as the through-wall distance from the inner radius of the RPV increases. The exponential coefficient adopted (-0.24) assumes that fluence attenuates at the same rate as displacements per atom (DPA) (a conservative assumption). A recent review of attenuation models [English 02] concluded that while the RG1.99R2 attenuation model is widely regarded as conservative, no better alternative model exists at the current time.

7.7 Crack Initiation Model

The crack initiation model is itself composed of the following major components:

- Fracture driving force model
  - LEFM driving force
  - Warm pre-stress
- Crack initiation resistance model
  - Unirradiated cleavage crack initiation toughness index temperature
  - Irradiation-induced shift in the cleavage crack initiation toughness index temperature
  - Cleavage crack initiation fracture toughness transition behavior

The probability of a crack initiating is determined by comparing the fracture driving force ($K_{applied}$) and the crack initiation resistance (K_{Ic}). If $K_{applied}$ for a given set of conditions (i.e., a particular TH transient and a particular flaw) exceeds the minimum value of the K_{Ic} distribution, the conditional probability of crack initiation (*CPI*) takes on a value greater than zero, which is calculated by FAVOR. Conversely, if $K_{applied}$ for a given set of conditions falls below the minimum value of the K_{Ic} distribution then *CPI*=0 (exactly zero, not a very small number).

In the following two subsections, we discuss the key features of the crack initiation model (Section 7.7.1) and the major differences between the current crack initiation model and that used in previous investigations of PTS risk (Section 7.7.2) [SECY-82-465, ORNL 85a, ORNL 85b, ORNL 86]. [***EricksonKirk-PFM***] provides a detailed discussion of the crack initiation model.

7.7.1 Key Features

7.7.1.1 Fracture Driving Force Model

Warm pre-stress (WPS) effects were first noted in the literature in 1963 [Brothers 63]. These investigators reported (as have many since them)

that the apparent fracture toughness of a ferritic steel can be elevated in the fracture mode transition regime if the specimen is first "pre-stressed" at an elevated temperature. Once a specimen is subjected to a certain $K_{applied}$ and has not failed, the temperature can be reduced and the specimen will remain intact despite the fact that the process of reducing the temperature has also reduced the initiation fracture toughness (K_{Ic} or K_{Jc}) to values smaller than $K_{applied}$. In the past four decades, the physical mechanisms responsible for the WPS effect have been identified, studied extensively, and validated.

The types of loading that produce PTS challenges are characterized (generally) by a rapid cooldown on the inside the RPV. This type of loading produces values of $K_{applied}$ that initially increase, but later decrease as the transient progresses. Thus, depending upon the specifics of the transient (temperature gradients, flaw location, and so on) WPS may be effective, thereby preventing initiation of a cleavage crack even though $K_{applied}$ exceeds K_{Ic}. Nonetheless, to date, investigations of PTS have not included WPS as part of the PFM model [SECY-82-465, ORNL 85a, ORNL 85b, ORNL 86] for the following two reasons:

(1) TH transients were previously represented as smooth variations of both pressure and temperature with time. However, data taken from operating nuclear plants demonstrate that actual TH transients are not always so well behaved. This created the possibility that the short duration fluctuations of pressure and/or temperature with time characteristic of real transients might nullify the beneficial effect of WPS while the companion idealized transient might show WPS to be effective.

(2) In the past, the probabilistic risk assessment (PRA) models of human reliability (HR) were not sufficiently sophisticated to capture the potential for plant operators to repressurize the primary system as part of their response to an overcooling event. Since such a repressurization would usually nullify the benefit of WPS, it was viewed as nonconservative to account for the benefit produced by WPS within a model that may also ignore the potentially deleterious effects of operator actions.

This reevaluation of the PTS Rule features both more realistic representations of the TH transients and a much more sophisticated PRA/HR models that consider explicitly both acts of omission and commission on the part of plant operators. Consequently, we have incorporated WPS effects into the PFM model. Thus, in this model the following two requirements must ***both*** be met for a crack to initiate:

Eq. 7-1 $$K_{applied} \geq K_{Ic(min)}$$
$$dK_{applied}/dt > 0$$

7.7.1.2 Crack Initiation Resistance Model

Our model of the resistance of ferritic steels to cleavage crack initiation includes the following characteristics:

- a temperature dependency of fracture toughness that is universal to all ferritic steels and is uninfluenced by irradiation
- a scatter in fracture toughness that is universal to all ferritic steels and is not influenced by irradiation
- a finite lower bound to the distribution of (scatter in) crack initiation toughness values (i.e., a value of fracture driving force below which cleavage fracture *cannot* occur)
- an irradiation damage model that recognizes that the effects of irradiation are purely athermal (i.e., affecting *only* the position of the fracture toughness transition curve on the temperature axis)

These characteristics are all motivated by an understanding of the physical processes responsible for cleavage fracture. While the numerical coefficients of our model are obtained empirically (i.e., obtained by fitting toughness data) the functional forms of the fits are physically motivated. This physical basis provides an additional benefit in that it helps provide assurance that the models apply to all

conditions of interest (i.e., to a variety of RPV steels and welds subject to range of irradiation conditions.

Our physical understanding of cleavage fracture also provides important guidance regarding how the uncertainty in fracture toughness should be modeled. Specifically, it is recognized that the distribution of non-coherent particles throughout the BCC iron lattice establishes the scatter in K_{Ic} and K_{Jc} data [Natishan 01, EricksonKirk 04]. It is possible, at least in principle, to know if a non-coherent particle exists at a particular point in the matrix, or not. This might suggest an epistemic nature to K_{Ic} and K_{Jc} scatter, were it not for the fact that K_{Ic} and K_{Jc} do not exist as point properties. K_{Ic} and K_{Jc} values always have an associated size scale, that being the plastically deformed volume. Upon loading, the presence of the crack elevates the stress state along the entire length of the crack front to the point that dislocations begin to move in the surrounding volume of material, which contains a distribution of dislocation barriers (e.g., non-coherent particles, grain boundaries, twin boundaries, etc.). Sufficient accumulation of dislocations at a barrier can elevate the local stress-state sufficiently to initiate a crack in the barrier, and, if the criteria for fracture are satisfied, propagate the crack through the entire surrounding test specimen or structure. Thus, the existence of a particular dislocation barrier at a particular location does not control K_{Ic} and K_{Jc}. Rather K_{Ic} and K_{Jc} are controlled by the *distribution* of these barriers throughout the lattice, and how this *distribution* interacts with the elevated stresses along the crack front. Since the distribution of these barriers throughout the lattice is random and occurs at a size-scale below that considered by the crack initiation toughness model, the uncertainty in K_{Ic} and K_{Jc} is irreducible. For this reason, the uncertainty in K_{Ic} is modeled as aleatory in FAVOR [***Williams***].

Beyond the aleatory uncertainty in K_{Ic}, our model of crack initiation toughness accounts for uncertainties in both the model and in the input parameters that are epistemic in nature. The major epistemic model uncertainty is the RT_{NDT} bias correction, which is discussed in the next section, because this represents a major change in the crack initiation model relative to that adopted in previous investigations of PTS. Epistemic uncertainties in input data (i.e., Cu, Ni, and P content, initial RT_{NDT}, and un-irradiated CVN upper-shelf energy) are accounted for and propagated through the FAVOR calculation. While the mean values of these distributions are the values the licensees have docketed [RVID2], the statistical distributions assumed to exist around these mean values were derived from *all data available* for the entire population of RPV-grade ferritic steels and their weldments. Consequently, these distributions overestimate (sometimes significantly so) the degree of uncertainty in these input variables relative to that which would characterize a *particular* weld, plate, or forging that would exist in the beltline of a *particular* PWR. While plant-specific studies might appropriately adopt less-scattered distributions, we have used generic distributions of the input variables to support our goal of developing a revision to 10 CFR 50.61 that applies to all PWRs.

7.7.2 Major Changes

In this section, we summarize the major changes between the calculational models adopted here and those used to support the current version of 10 CFR 50.61.

7.7.2.1 Fracture Driving Force Model

As discussed in Section 7.7.1.1, our models incorporate the effects of WPS, whereas previous studies of PTS have not. Adopting a WPS model can reduce the TWCF estimated for certain classes of transients. For example, the TWCF estimated for a primary side pipe break will be significantly smaller when the effects of WPS are considered, while the TWCF estimated for a stuck-open valve that recloses later during the transient (thereby repressurizing the primary system) may not be affected by WPS at all. In plant analyses of Oconee Unit 1 based on a complete set of transients (i.e., considering the potential for vessel failure from all potential PTS

precursors), inclusion of WPS in the model reduces the estimated TWCF by between a factor of 2½ and 3 [Dickson 03]. Dickson's results show that while the degree of "benefit" associated with adopting a WPS model depends on the transients considered to produce PTS risk it is reasonably insensitive to the degree of embrittlement.

7.7.2.2 Crack Initiation Resistance Model

Relative to the models used in the studies that established the technical basis to the current PTS Rule [SECY-82-465, ORNL 85a, ORNL 85b, ORNL 86], our model has the following *major* differences (see [***EricksonKirk-PFM***] for a comprehensive discussion of *all* differences):

(1) Consideration of Systematic Material Property and Fluence Variations throughout the Beltline Region: In previous studies, the known systematic variations of material properties and fluence throughout the beltline region were treated in a highly simplified fashion. Specifically, the effect of radiation damage on each major region (i.e., each plate, weld, or forging) of the vessel was assessed assuming that the entire region was subjected to the maximum fluence occurring anywhere in the region. This approach led to significant overpredictions of the embrittlement of the vessel, and consequent overestimates of the PTS risk. These conservatisms are absent from our model.

(2) Treatment of Fracture Toughness Scatter as Aleatory: The aleatory model of fracture toughness uncertainty described in Section 7.7.1.2 differs from the epistemic treatment of toughness uncertainty adopted in all pervious probabilistic studies of PTS. In these studies the result of a particular trial in the calculation was the prediction that the vessel *had* or *had not* failed. While this epistemic treatment is inconsistent with our current understanding of the physics of cleavage fracture, the difference in the mean TWCF estimates produced by these two different approaches is small (all other factors being held constant).

(3) RT_{NDT} Bias Correction: While the restrictions on model development detailed in Section 3.1.1 require that the basis of our model be non-toughness metrics (i.e., RT_{NDT}) our model recognizes that RT_{NDT} is not a direct measure of the fracture toughness transition temperature. Indeed RT_{NDT} is by intention a conservative approximation to the true fracture toughness transition temperature, overestimating this value (an implicit conservatism) by 65°F (18°C) on average, and up to 200°F (93°C) in some cases. Our model removes this conservative bias (on average), but in the process, introduces a non-physical model uncertainty. This model uncertainty, which cannot be removed as long as we rely on RT_{NDT}-based metrics, should be regarded as an implicit conservatism in our results. This bias correction significantly reduces the estimated annual through-wall cracking frequency.

7.7.2.3 Method for Estimating Vessel Crack Initiation Probability from the Probability of Initiation of Individual Cracks in the Vessel

Our treatment of the uncertainty in crack initiation fracture toughness (K_{Ic}) as aleatory necessitates use of a different methodology for estimating the probability of crack initiation in the vessel from the probabilities of initiation of the many individual cracks throughout the vessel from that adopted in the calculations used in [SECY-82-465][§§]. In previous probabilistic studies of PTS, the uncertainty in K_{Ic} was modeled as being epistemic, meaning that for any individual simulation, there existed a single value of K_{Ic}. Consequently, if the probabilistic computer code simulated that the applied fracture driving force ($K_{applied}$) resulting from a PTS transient ever exceeded K_{Ic} for any of the

[§§] The discussion in this section also applies to the mathematical combination the probability of individual cracks propagating through-wall to estimate the probability of the vessel developing a through-wall crack.

flaws in the vessel, the vessel failure probability was set to 1 (a certainty) and further calculations for that vessel were not performed because a vessel cannot fail twice. When K_{Ic} uncertainty is correctly modeled as being aleatory (as it is in our model), a different approach is needed because the result of each simulation run is not vessel non-failure (probability 0) or vessel failure (probability 1), but rather vessel non-failure (probability 0) or vessel failure *probability* ($0 <$ probability ≤ 1; in practical terms vessel failure probability is usually a very small number that is ***not*** close to 1). In this situation, the appropriate representation of the vessel failure probability is the complement (meaning the difference from 1) of the joint (meaning combined) probability of non-failure of all of the flaws in the vessel [Fang 03], which can be expressed mathematically as follows:

Eq. 7-2 $$P_{FAIL(VESSEL)} = 1 - \prod_{j=1}^{n} \left(1 - P_{FAIL(j)}\right)$$

where n is the total number of flaws simulated to exist in the pressure vessel. This equation can be stated in words as follows: *the probability that the vessel will fail is 1 minus the probability that all of the cracks in the vessel do not fail*, or, even more simply: *in order for the vessel to not fail all of the cracks in it must not fail.*

During the many public meetings that have been held during the course of the PTS reevaluation project, concerns have been expressed that this methodology for estimating the vessel failure probability is both inappropriate and overly conservative. The following alternative probability formula has been proposed:

Eq. 7-3 $$P_{FAIL(VESSEL)} = \underset{j=1}{\overset{n}{MAX}} \left(P_{FAIL(j)}\right)$$

This equation states that the failure probability of the vessel is the maximum of the individual failure probabilities associated with the many individual cracks in the vessel. The appropriateness of Eq. 7-2 rather than Eq. 7-3 when estimating the total probability associated with system failures (vessels) that might result from many individual causes (cracks) can be easily understood by way of analogy. Consider the "system" to be an individual human life and consider the "failure" to be death. Below, we provide two examples to illustrate the differences between Eq. 7-2 and Eq. 7-3, and the appropriateness of Eq. 7-2:

Example 1: Hypothetical individual #1 leads a very controlled life and (so) is subject to only one cause of death (cancer). The individual's annual risk of dying of cancer is 2%. In this situation, this individual's total annual risk of death is estimated to be 2% by either Eq. 7-2 or by Eq. 7-3.

Example 2: Hypothetical individual #2 is less careful than hypothetical individual #1 and (so) is at risk from more than one cause of death. The individual's annual risk of dying from any one of four causes is as follows: cancer=2%, AIDS=1%, skydiving=½%, gunshot=¼%. Clearly individual #2 has a greater annual death risk than individual #1, yet Eq. 7-3 estimates their annual death risks to be identical: MAX(2%, 1%, ½%, ¼%), or 2%. Conversely, Eq. 7-2 estimates individual #2's annual death risk to be {1-(1-0.02)*(1-0.01)*(1-0.005)*(1-0.0025)}, or 3.7%.

It can also be noted that for the particular situation of interest here (PTS-induced failures of nuclear RPVs containing cracks), the numerical differences between the failure probabilities estimated by Eq. 7-2 and Eq. 7-3 is actually very small because, as illustrated in Figure 7.5, for the great majority of the time, only one crack in a vessel has a probability of through-wall cracking that exceeds zero. It was for this reason, that Meyer assessed the differences between Eq. 7-2 and Eq. 7-3 to be practically insignificant [Meyer 03].

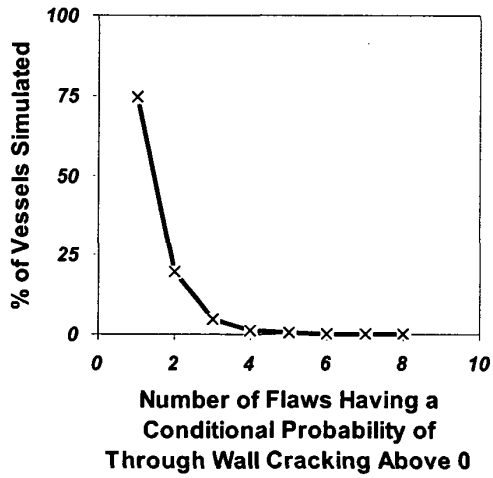

Figure 7.5. Number of flaws simulated that have a conditional probability of through-wall cracking that exceeds zero (Oconee at 60 EFPY).

7.8 Through-Wall Cracking Model

Provided that the results of a particular trial for a particular simulated flaw result in an estimation of $CPI > 0$, FAVOR will check to see how far the simulated crack will propagate into the vessel wall before it arrests permanently (if it arrests at all). The through-wall cracking model is itself composed of the following component models:

- Fracture driving force
  - LEFM driving force
- Crack growth resistance
  - cleavage crack arrest
  - upper shelf ductile tearing model
  - property gradient model

The probability of through-wall cracking is determined by comparing the fracture driving force ($K_{applied}$) to the resistance to further crack growth, which is expressed as a value of cleavage crack arrest toughness (K_{Ia}). Additionally, once a propagating crack has arrested the potential for re-initiation at some later time in the transient is assessed relative to the material's resistance to crack initiation in either cleavage (K_{Ic}) or by ductile tearing ($K\{J_{Ic}\}$, and the associated *J-R* curve). For each simulation where FAVOR calculates a value of $CPI > 0$, it then conducts 100 deterministic through-wall cracking analyses. The outcome of each of these deterministic simulations is either that the crack propagates all the way through the thickness of the vessel[***], or that the crack arrests before it reaches the outer diameter. The percentage of the trials that result in through-wall cracking is then multiplied by the *CPI* value to estimate the *CPTWC*.

In the following two subsections, we discuss the key features of the through-wall cracking model (Section 7.8.1) and the major differences between our model and that used in previous investigations of PTS risk (Section 7.8.2) [SECY-82-465, ORNL 85a, ORNL 85b, ORNL 86]. These sections address only the crack growth resistance models because the fracture driving force models are the same as used for crack initiation. [***EricksonKirk-PFM***] provides a detailed discussion of the through-wall cracking model.

7.8.1 Key Features

Our model of the resistance of ferritic steels to through-wall cracking includes both a cleavage crack arrest model and a model for re-initiation of a crack by ductile tearing on the upper shelf[†††]. These models include the following characteristics:

- Crack arrest toughness model
  - a temperature dependency of crack arrest toughness that is universal to all ferritic steels and is not influenced by irradiation
  - a scatter in crack arrest toughness that is universal to all ferritic steels and is not influenced by irradiation

[***] In practice, when the crack extends 90% of the way through the wall thickness the vessel is considered to have failed.

[†††] The through-wall cracking model also accounts for the possibility of re-initiation in cleavage, but for these purposes the crack initiation model described previously in Section 7.7 is used.

- a finite lower bound to the distribution of (scatter in) crack arrest toughness values (i.e., a value of fracture driving force below which cleavage fracture *cannot* occur)
- a model that positions the crack arrest transition temperature depending on the crack initiation transition temperature, and recognizes that the temperature differential between the crack initiation and crack arrest transition temperatures depends on the amount of prior hardening (i.e., irradiation damage) experienced by the material

- Upper shelf ductile initiation and tearing model
  - a temperature dependency of upper-shelf toughness that is universal to all ferritic steels and is not influenced by irradiation
  - a scatter in upper-shelf toughness that is universal to all ferritic steels and is not influenced by irradiation
  - a linkage between the magnitude of the fracture toughness on the upper shelf and the fracture toughness transition temperature

These characteristics are all motivated by an understanding of the physical processes responsible for both cleavage crack arrest and for ductile crack initiation on the upper shelf. While the numerical coefficients of our models are obtained empirically (i.e., obtained by fitting toughness data), the functional forms of the fits are physically motivated. This physical basis provides an additional benefit in that it helps provide assurance that the models apply to all conditions of interest (i.e., to a variety of RPV steels and welds subject to range of irradiation conditions).

Our physical understanding of both cleavage crack arrest and of ductile crack initiation also provides important guidance regarding how the uncertainty in fracture toughness should be modeled. As was the case for cleavage crack initiation toughness, it is recognized that the physical processes responsible for both cleavage crack arrest and for ductile crack initiation make the uncertainty in these toughness values aleatory in nature [***EricksonKirk-PFM***], and it is so modeled in FAVOR [***Williams***].

7.8.2 Major Changes

Relative to the models used in the studies that established the technical basis to the current PTS Rule [SECY-82-465, ORNL 85a, ORNL 85b, ORNL 86], our model has the following *major* differences (see [***EricksonKirk-PFM***] for a comprehensive discussion of *all* differences):

(1) Allowance of Ductile Tearing and Inclusion of Crack Arrest Resistance at $K_{applied}$ Values Above 200 ksi$\sqrt{in}$ (220 MPa$\sqrt{m}$): In all former studies of PTS (including our own study reported in [***Kirk 12-02***]) the resistance to crack arrest was truncated at 200 ksi$\sqrt{in}$ (220 MPa$\sqrt{m}$) because this is the highest value allowed by the ASME code K_{Ia} curve. However, ample evidence from large-scale experiments exists demonstrating that crack arrest above 200 ksi$\sqrt{in}$ (220 MPa$\sqrt{m}$) does occur, indicating the inappropriateness and over-conservatism of the 200 ksi$\sqrt{in}$ (220 MPa$\sqrt{m}$) limit. Moreover, no allowance was ever made in former studies of the possibility for an arrested crack to re-initiate by ductile tearing on the upper shelf despite the fact that the resistance to crack initiation on the upper shelf ranges between 100 and 200 ksi$\sqrt{in}$ (110-220 MPa$\sqrt{m}$) for ferritic RPV steels both before and after irradiation. We have eliminated this apparent oversight in our through-wall cracking model. As shown in Figure 7.6, the combined effect of these two changes is a reduction in the TWCF by a factor of 4–5 (at lower levels of embrittlement) down to a reduction factor of ~1.5 as embrittlement increases. Allowing cracks to arrest at $K_{applied}$ values above 200 ksi$\sqrt{in}$ has resulted in cracks being arrested at shallower depths, which in turn makes re-initiation by either cleavage or ductile fracture more difficult. Thus, removing the conservatism of the 200 ksi$\sqrt{in}$ (220 MPa$\sqrt{m}$) limit on K_{Ia} more than

compensated for the non-conservatism associated with assuming that re-initiation in a ductile mode cannot occur.

(2) A Separation between the K_{Ic} and K_{Ia} Curves that Depends on the Degree of Irradiation Embrittlement: In all studies of PTS risk predating this reevaluation, the temperature separation between the K_{Ic} and K_{Ia} transition curves was held fixed irrespective of the material condition, as has always been the practice for the ASME K_{Ic} and K_{Ia} curves. However, because ferritic steels harden to an absolute limit [Wagenhofer 01], the separation between the two curves depends upon the degree to which the material is hardened, with more hardened (more irradiated) materials having smaller separations [Kirk 02a]. This is also supported by ample empirical evidence [Wallin 98b]. We have not performed a sensitivity study to assess the effect of this model change. However, comparison of the temperature differential between the K_{Ic} and K_{Ia} curves adopted by our current model (see curve of Figure 7.7) with the constant temperature differential of ~30°C (~86°F) previously assumed (i.e., the temperature separation between the ASME K_{Ic} and K_{Ia} curves) demonstrates our new model reduces the crack arrest capacity of higher toughness materials (i.e., materials having a T_o value of ~60°C (~140°F) or less) because the greater K_{Ic} to K_{Ia} curve separation adopted by our model reduces the of value of K_{Ia} at a fixed K_{Ic}. Conversely, the crack arrest capacity of more embrittled materials (i.e., materials having a T_o value of ~60°C (~140°F) or more) is greater in our model than it is in the ASME model.

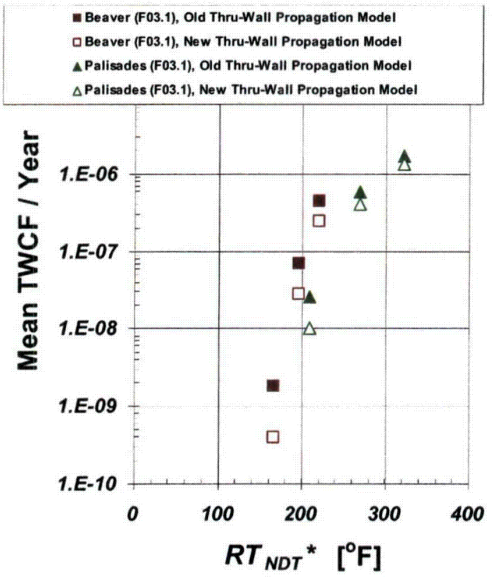

Figure 7.6. Combined effects of allowing K_{Ia} to exceed 200 ksi√in and allowing for ductile crack re-initiation on the upper shelf. Open points show TWCF results when K_{Ia} is allowed to exceed 200 ksi√in and ductile crack re-initiation is permitted. RT_{NDT}* is defined in [*Kirk 12-02*].

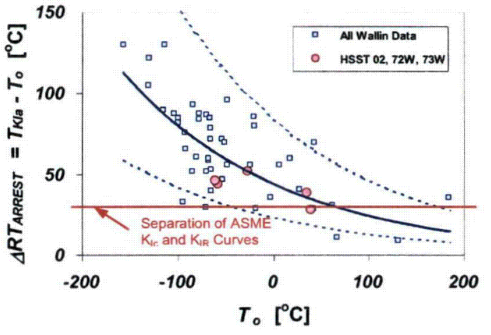

Figure 7.7. Comparison of temperature separation between crack initiation and crack arrest toughness transition curves assumed in our current calculations (blue curve) with the constant separation of ~30°C (~86°F) assumed by previous calculations

7.9 Probabilistic Fracture Mechanics Code FAVOR

7.9.1 Implementation of PFM Model

As shown in Figure 7.8, FAVOR is composed of three computational modules: (1) a deterministic load generator (**FAVLoad**), (2) a Monte Carlo PFM module (**FAVPFM**), and (3) a post-processor (**FAVPost**). Figure 7.8 also indicates the nature of the data streams that flow through these modules.

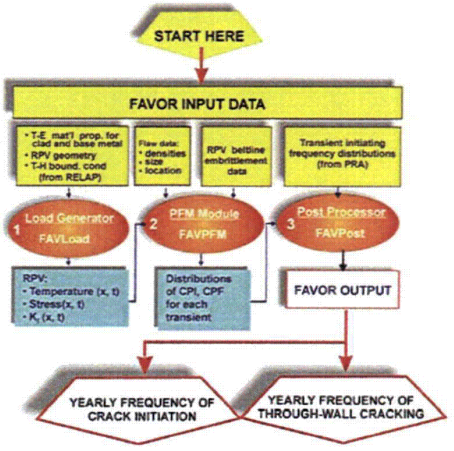

Figure 7.8. FAVOR data streams flow through three modules: (1) FAVLoad, (2) FAVPFM, and (3) FAVPost

FAVLoad takes as input the time histories of pressure, temperature, and heat transfer coefficient defined by the RELAP TH analysis. These inputs are used along with a 1D transient heat conduction equation to estimate the time-dependent variation of temperature through the vessel wall. These time-dependent temperature profiles are used, along with the RELAP pressure history, in a linear elastic stress analysis to estimate the time history of applied-K_I, which is passed to FAVPFM for further analysis.

The FAVPFM module implements the logical specification of the PFM model within a series of nested loops illustrated in Figure 7.9. These loops step through the TH time history and implement the Monte-Carlo trials necessary to estimate the conditional probabilities of crack initiation and of though wall cracking. The probabilities estimated by FAVOR (complete with uncertainties) are *conditional* in the sense that, within the FAVPFM module, the TH transients are assumed to occur.

The FAVPFM module provides the capability to model the variation of radiation damage in the *beltline region* of an RPV with as much detail as the analyst considers necessary. Only that portion of the beltline that is proximate to the active core need be modeled because the fast-neutron flux, and thus the radiation damage, drops to nearly zero within a foot beyond the fuel region. Within this region (active core ±1-ft. (0.3-m), the vessel is represented as a combination of "major regions," with each major region representing a different plate, weld, or forging each having (potentially) a unique combination of mean copper content, mean nickel content, mean phosphorus content, and unirradiated RT_{NDT}. Each major region may be divided into as many "sub-regions" as the analyst feels are necessary to represent accurately both the axial and azimuthal variation of fluence. Sufficient discretization is adopted so that each sub-region is effectively subjected to the same fluence throughout. In this way, the complex variation of embrittlement throughout the vessel wall that is caused by variations in both material and radiological conditions is represented to the model. It should be noted that this material/radiological model is a considerably more accurate representation of reality than the models adopted in the calculations performed to support SECY-82-465 and the IPTS studies. In these earlier calculations, the entire vessel was presumed to be made out of the most irradiation-sensitive material, and all of this material was assumed to be subjected to the peak fluence that occurred anywhere in the vessel.

The last FAVOR module, FAVPost, combines the conditional initiation and through-wall cracking probabilities and combines these, through a matrix multiplication, with the frequency histograms for each TH sequence provided by the PRA analyses. In this way, the complete distribution of TWCF (per operating year) is estimated.

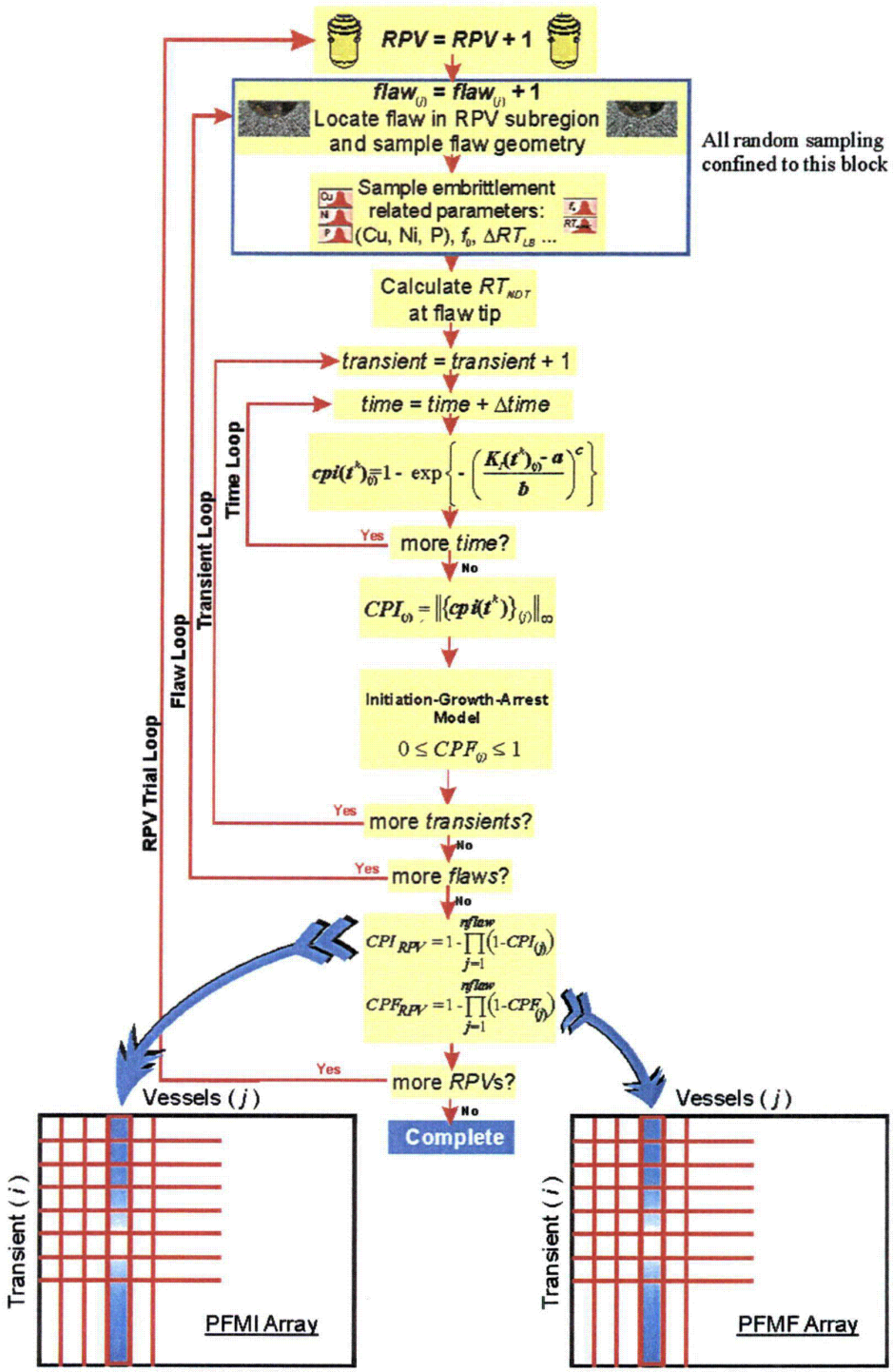

Figure 7.9. **Flow chart for improved PFM model implemented in FAVPFM showing the four primary nested loops – (1) *RPV Trial Loop*, (2) *Flaw Loop*, (3) *Transient Loop*, and (4) *Time Loop***

7.9.2 Discretization of the Reactor Pressure Vessel

FAVOR utilizes discretizes the RPV beltline into one "major regions" for each axial weld, circumferential weld, plate, and forging. The major regions are further subdivided into iso-fluence "subregions." To model accurately the complex variation of fluence with azimuth and axial location (see Figure 7.10) a large number of sub-regions was necessary (15280, 19651, and 67076 subregions for Beaver Valley, Oconee, and Palisades, respectively). The neutron fluence maps were provided for 32 and 40 EFPY were used, and were linearly extrapolated to estimate fluence for longer operational durations.

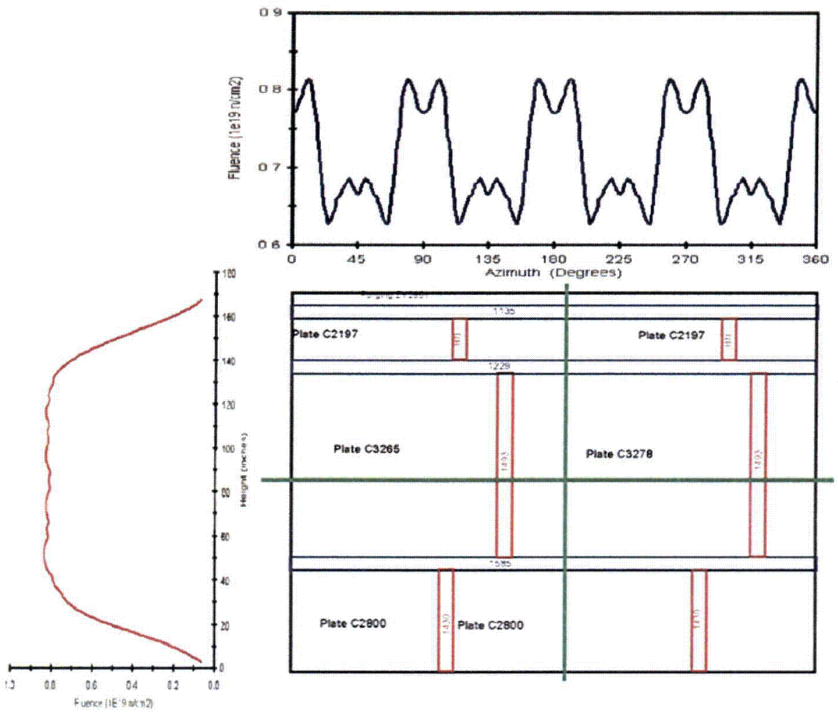

Figure 7.10. Rollout diagram of beltline materials and representative fluence maps for Oconee Unit 1

7.10 Experimental Validation of Linear Elastic Fracture Mechanics

Extensive experimental/analytical investigations performed at ORNL during the 1970s and 1980s examined the accuracy with which LEFM models could be expected to predict the failure of nuclear RPVs subjected to both simple loadings (pressure only) and to much more complex loadings (PTS conditions) [Cheverton 85a, Cheverton 85b]. These investigations all featured tests on thick-section pressure vessels (see Figure 7-11), and aimed to reproduce, as closely as practical in a laboratory setting, the conditions that characterize thermal shock of a nuclear RPV. These conditions include the following:

- fracture initiation from small flaws
- severe thermal, stress, and material toughness gradients
- biaxial loading
- effects of cladding (including residual stresses)
- conditions under which warm pre-stress may be active

- combined stress and toughness gradient conditions that can promote crack initiation, arrest, re-initiation, and re-arrest all during the same transient
- due to these various gradients, the possibility of conversion of fracture mode from cleavage to ductile and back again all during the same TH transient

The three test series were as follows:

- The first series of tests employed ten intermediate test vessels (ITVs), three with cracks located at a cylindrical nozzle and seven with cracks located remote from any geometric discontinuities. These tests were aimed at investigating the ability of LEFM to predict the fracture response of thick section vessels containing relatively deep flaws (20 to 83% of the 6-in. (152.4 mm) vessel wall) at test temperatures ranging from lower shelf to upper shelf. A variety of nuclear grade RPV plates, forgings, and weldments were tested.
- The second series of tests comprised eight thermal-shock experiments (TSEs). The purpose of these experiments was to investigate the behavior of surface cracks under thermal-shock conditions similar to those that would be encountered during a large-break loss of coolant accident (LBLOCA) (i.e., a rapid cooldown in the absence of internal pressure).
- The third series of tests included two experiments that subjected ITV specimens to concurrent pressure and thermal transients. These "pressurized thermal shock experiments," or PTSEs, sought to simulate the effects of a rapid cooldown transient combined with significant internal pressure. Thus, these experiments simulated TH conditions characteristic of smaller break LOCAs.

These investigations support the following conclusions:

- ITV Experiments:
  - LEFM analyses very closely predicted actual fracture pressures for thick-wall pressure vessels.
  - Methods for calculating fracture toughness from small specimens were successfully used in applications of fracture analysis of thick flawed vessels.
- Thermal Shock Experiments (TSEs):
  - Multiple initiation-arrest events with deep penetration into the vessel wall were predicted and observed.
  - Surface flaws that were initially short and shallow were predicted and observed to grow considerably in length before increasing significantly in depth.
  - Warm pre-stress was observed to limit crack extension through the wall under LOCA conditions.
  - Small-specimen fracture mechanics data successfully predicted the fracture behavior of thick pressure vessels.
  - Crack arrest occurred in a rising stress field.
- Pressurized Thermal Shock Experiments (PTSEs):
  - Warm pre-stress is effective at inhibiting crack initiation for conditions under which crack initiation would otherwise be expected (i.e., $K_{applied} > K_{Ic}$).
  - Crack arrest toughness values (K_{Ia}) inferred from conditions prototypic of PTS loading agree well with other experimental measurements, suggesting the transferability of laboratory toughness data to structural loading conditions.

- LEFM predictions of crack initiation, growth, and arrest behavior successfully captured the response of the vessel to the transient; however some details were not exactly predicted (two initiation-run-arrest events were predicted whereas one was observed).

With regard to this final bullet item, it should be noted that exact agreement between deterministic predictions and individual experiments cannot be expected when the physical processes that underlie those experiments produce large aleatory uncertainties (as is the case with K_{Ic} and K_{Ia} data; see Sections 7.7.1.2 and 7.8.1, respectively). Such disagreement does not in itself condemn the methodology, but rather reveals that the precision of any single prediction is limited by the precision in our knowledge of the controlling material properties.

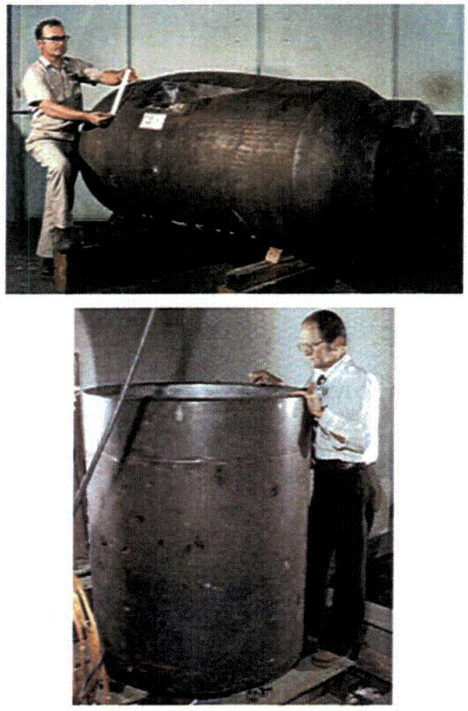

Figure 7-11. Test vessels used in the ITV and PTSE test series (top) and in the TSE test series (bottom)